DEPARTMENT OF MECHANICAL ENGINEERING
SCHOOL OF ENGINEERING
OLD DOMINION UNIVERSITY
NORFOLK, VIRGINIA 23508

NUMERICAL STUDY OF HYDROGEN-AIR SUPERSONIC COMBUSTION
BY USING ELLIPTIC AND PARABOLIZED EQUATIONS

By

Tawit Chitsomboon, Graduate Research Assistant

Surendra N. Tiwari, Principal Investigator

Progress Report
For the period December 1, 1985 to May 31, 1986

Prepared for the
National Aeronautics and Space Administration
Langley Research Center
Hampton, Virginia 23665

August 1986

OLD DOMINION UNIVERSITY RESEARCH FOUNDATION

DEPARTMENT OF MECHANICAL ENGINEERING
SCHOOL OF ENGINEERING
OLD DOMINION UNIVERSITY
NORFOLK, VIRGINIA 23508

NUMERICAL STUDY OF HYDROGEN-AIR SUPERSONIC COMBUSTION
BY USING ELLIPTIC AND PARABOLIZED EQUATIONS

By

Tawit Chitsomboon, Graduate Research Assistant

Surendra N. Tiwari, Principal Investigator

Progress Report
For the period December 1, 1985 to May 31, 1986

August 1986

NUMERICAL STUDY OF HYDROGEN-AIR SUPERSONIC COMBUSTION
BY USING ELLIPTIC AND PARABOLIZED EQUATIONS

By

Tawit Chitsomboon[1] and Surendra N. Tiwari[2]

ABSTRACT

The two-dimensional Navier-Stokes and species continuity equations are used to investigate supersonic chemically reacting flow problems which are related to scramjet-engine configurations. A global two-step finite-rate chemistry model is employed to represent the hydrogen-air combustion in the flow. An algebraic turbulent model is adopted for turbulent flow calculations. The explicit unsplit MacCormack finite-difference algorithm is used to develop a computer program suitable for a vector processing computer. The computer program developed is then used to integrate the system of the governing equations in time until convergence is attained.

The chemistry source terms in the species continuity equations are evaluated implicitly to alleviate stiffness associated with fast chemical reactions. The block mono-diagonal system of algebraic equations, resulting from treating the source terms implicitly, can be inverted efficiently on vector processing computers. Both premixed and nonpremixed reacting flows are solved. Some of the results are compared with those using a complete-reaction chemistry model. It is found that the finite-rate model predicts the same trends as the complete-reaction model, but the former allows lesser extent of combustion.

The problems solved by the elliptic code are re-investigated by using a set of two-dimensional parabolized Navier-Stokes and parabolized species

---

[1] Graduate Research Assistant, Department of Mechanical Engineering and Mechanics, Old Dominion University, Norfolk, Virginia 23508.
[2] Eminent Professor, Department of Mechanical Engineering and Mechanics, Old Dominion University, Norfolk, Virginia 23508.

equations. The thermo-chemical and turbulence models utilized are the same
as used in the fully elliptic procedure (with proper modifications). A
linearized fully-coupled fully-implicit finite-difference algorithm is used
to develop a second computer code which solves the governing equations by
marching in space rather than time, resulting in a considerable saving in
computer resources. Results obtained by using the parabolized formulation
are compared with the results obtained by using the fully-elliptic equa-
tions. The comparisons indicate fairly good agreement of the results of the
two formulations.

FOREWORD

This is a progress report on the research project "Analysis and Computation of Internal Flow Field in a Scramjet Engine." The period of performance on this research was December 1, 1985 through May 31, 1986. The work was supported by the NASA Langley Research Center (Computational Method Branch of the High-Speed Aerodynamics Division) through research grant NAG-1-423. The grant was monitored by Dr. Ajay Kumar of the High-Speed Aerodynamics Branch.

TABLE OF CONTENTS

TABLE OF CONTENTS - Continued

LIST OF TABLES

LIST OF FIGURES

TABLE OF CONTENTS - Concluded

LIST OF FIGURES - Concluded

LIST OF SYMBOLS

a	speed of sound
a_i, b_i	constant for evaluating the specific heat of the (i)th species
C_c	parameter for improving robustness of the parabolized algorithm
C_E, C_I	explicit, implicit smoothing coefficients for the parabolized algorithm
C_i'	reaction rate of the (i)th species on molar basis
C_p	specific heat at constant pressure
D	effective mass diffusion coefficient
e_t	total internal energy
E, F	flux vectors in ξ, η directions
E	activation energy
f_i	mass fraction of the (i)th species
h	static enthalpy
H	total enthalpy
H_i^0	enthalpy of formation at 0 K of the (i)th species
J	Jacobian of coordinate transformation
k_{fi}, k_{bi}	forward, backward reaction rate coefficients for the (i)th reaction equation
K_i	equilibrium constant for the (i)th species
Le	Lewis number
M_i	molecular weight of the (i)th species
p	pressure
Pr, Pr_t	laminar, turbulent Prandtl number
q	dependent variable vector; heat flux
R	gas constant; residual
Re	Reynolds number

t	time
T	temperature
u, v	velocities in the x, y directions
W_i	reaction rate of the (i)th species on mass basis
x, y	physical coordinates
α	thermal diffusivity
ξ, η	computational coordinates
μ, μ_t	laminar, turbulent viscosities
ν	kinematic viscosity
ρ	mixture density
ρ_i	density of the (i)th species

1. INTRODUCTION

General background information and motivation for the present study are discussed in this section. Review of related literature is presented followed by specific objectives of the study.

1.1 Background

A comprehensive research program has been underway particularly at the NASA Langley Research Center to develop supersonic combustion ramjet (scramjet) engine for hypersonic aircraft cruising at Mach 5 and beyond [1-4].[*] Flow characteristics at these speeds dictate engine-airframe integration where the forebody of the vehicle is used to partially compress incoming air for the inlet of the engine which is mounted directly underneath and becomes an integral part of the vehicle. The aftbody of the vehicle, immediately downstream of the engine, is used as part of the nozzle to provide additional thrust. Hydrogen has been a strong candidate for fueling this type of engine due to its many desirable properties such as high specific impulse and cooling effect.

The engine module has a rectangular capture area with sweep of the sidewalls and a cut back cowl in order to provide flow spillage which allows the inlet to start at low flight speeds. The compression process in the inlet is completed by wedge-shaped struts which also provide multiple planes for injection of gaseous hydrogen fuel. The combustor has a diverging shape and employs varying amounts of parallel and perpendicular fuel injection from the sidewalls and the struts.

A cut-and-try procedure which is inevitable in the initial phase of experimentation has always proved to be expensive and time consuming

---

*The numbers in brackets indicate references.

especially for hypersonic flow research; this has led the way to numerical experimentation. In this study, the attention is directed on applying numerical techniques to compute a chemically reacting flow field through the scramjet engine.

Numerical investigation of a complex chemically reacting flow requires enormous computer resources, well-proven numerical algorithms and realistic chemical kinetics models. The advent of supercomputers such as the VPS-32 vector processing computer at the NASA Langley Research Center has alleviated some restrictions on the computer resource, provided the computer code is written to take advantage of the hardware of the computer. Advancements in numerical algorithms in the past decade have made numerical investigations more reliable research tools than ever before. Chemical kinetics of the hydrogen-air system are the most studied and understood phenomena, providing ample reliable data base for all levels of sophistication.

The flow field of a scramjet engine is quite complex. Shock waves emanating from the sidewalls and the struts leading edges are strong enough to separate the turbulent boundary layers in the inlet. Interactions of shock waves and expansion fans are also expected to be strong. The flow field near transverse fuel injectors is particularly complex. Blockage and deflection of the supersonic mainstream flow by the fuel jets give rise to an adverse pressure gradient which separates the turbulent boundary layer upstream of the injectors. The flow field in the combustor is further complicated by the highly turbulent mixing and exothermic reaction of hydrogen and air. Moreover, the efffect of combustion in the combustor could be felt upstream through the subsonic boundary layers which could degrade the performance of the inlet. Several injector-diameters downstream of the injector, however, the flow becomes less complex; a predominant flow direction

2

can be determined in which there is no flow separation.

To resolve all kinds of interaction discussed, the fully elliptic form of the governing partial differential equations must be used in the inlet and in the near field of the injectors. Flow in the rear section of the combustor and aftbody of the vehicle (where flow additionally expands) can be solved by a much less expensive parabolic or parabolized form of the governing equations since elliptic effects in the predominant flow direction are negligible in these regions.

1.2 Survey of Pertinent Literature

Nonreacting flows in various two- and three-dimensional inlet configurations were studied by Kumar [5-7]. In these studies, the fully elliptic form of the governing equations are employed for accurate representation of the flow field which involves separations due to shock-wave/boundary-layer interaction. The computer codes developed are highly efficient on the vector processing computers since they are fully vectorized. Limited success was reported by Chitsomboon and Tiwari [8] and Chitsomboon et al. [9] in using a parabolized form of the governing equations for solving non-reacting flow through the related configurations. Effect of gaseous fuel injection without combustion and with a complete combustion model were also investigated [10-11].

Incorporation of chemical reaction into a numerical scheme for solving fluid flow problems is quite an endeavor. First of all, a chemistry model compatible with the physical problem being solved must be selected. Depending on the rate of chemical reaction relative to the characteristic time of the fluid flow, the suitable chemistry model could be any one of the following models:

1. frozen flow model

2. finite rate model

3. equilibrium model

4. complete reaction model

In general, the finite-rate model is the most accurate one but it is also the most difficult to implement. More often than not, a compromise must be made as to the level of complexity of the chemistry model selected and the computer resources available.

Simple introductions to the physics and the mathematics of chemically reacting flow can be found in [12-15]. Over the past decade, a number of finite rate chemistry models for the hydrogen-air system have appeared in the literature. Rogers and Schexnayder [16] proposed as many as 60 reaction paths in their model; this is certainly one of the most complete representations of hydrogen-air reaction. Unfortunately, the enormous number of reaction paths and chemical species involved in the model do not lend themselves feasible for a numerical investigation, at least within the current capability of state-of-the-art computers. Intermediate-level models [17] reduce the reaction paths down to twenty-five and eight with the number of species of twelve and eight, respectively. Except for some inaccuracies during the ignition delay period, the eight-reaction model performs as well as the 25-path model. Although these models are considerable less tedious than the 60-path model, they are expected to be too costly to use for routine parametric studies especially if the fully elliptic governing equations were to be used. The global two-step chemistry model of Rogers and Chinitz [18] offers an alternative to numerical investigators since it is a finite rate model with only four species of reactants and products and with only two reaction paths. This model was deduced by fitting the temperature history

4

of a 28-reaction model [16] used in a series of constant-pressure stream-tube calculations. While there are a number of limitations to this model such as ignition phase inaccuracy and a tendency to overpredict the flame temperature, the model is considered to be appropriate for initial parametric study of overall mixing and extent of combustion.

It is the rule rather than the exception that incorporation of a finite rate chemistry model into a numerical scheme will yield a stiff system of governing differential equations. Stiffness arises from disparity in time scales of the governing equations and has its meaning only in the context of numerical or computational mathematics. From a mathematical view point, a system of equations is stiff if the eigenvalues of the coefficient matrix of its locally linear representation have negative real parts that are widely disparate [13]. From a practical perspective, the size of the time step of integration is severely limited by stability rather than accuracy when stiff phenomenon exists [19]. The disparity in time scales, in turn, is caused by wide differences in rates of chemical reaction of various species; usually the fastest reaction is the one that causes stiffness.

During transient period (or ignition delay period), some free radicals may be produced very rapidly for a very short duration of time; thereafter, they stay relatively unchanged at their equilibrium values since other reactions begin to consume them as soon as they are produced. It is paradoxical that stiffness occurs only when the rapid transient state has subsided [13, 20]. During the rapid transient period, small time steps must be used anyway in order to resolve the rapidly-changing temporal history and therefore, the system is not stiff since time step is limited by accuracy. During equilibrium period, rates of reactions slow down by several orders of magnitude and it is natural to use much larger time step (while still

maintaining accuracy) for economical reasons. Use of large time steps, however, will result in numerical instability because stability of the governing differential equations is still dictated by the smallest time scale. An eigenvalue analysis of a model problem clearly illustrates this point (see, e.g., Ref. 21).

Stiff phenomenon is studied extensively in the framework of ordinary differential equations (ODE) which are representative of the governing equations of a well-stirred reactor or a batch-chemistry system (systems with no spatial gradients) [19, 22-26]. In most cases, some form of implicitness is used to evaluate chemistry source terms in order to alleviate stiffness. Some of the most popular stiff ODE solvers are those of Hindmash [23-24]. These solvers are based on the methods of Gear [25-26] which, in turn, contain different implementations of the Adams formulae. When applied to flow problems, an Adams-based algorithm was found to be inferior to the four-step Runge-Kutta algorithm [27].

In light of the above discussion, it is realized that fully explicit numerical methods cannot be used to time integrate the stiff governing equations of chemically reacting flow due to the prohibitively small time step required to ensure stability. If only a steady state solution is sought, implicit methods could be used with no restriction on time-step size. Use of fully implicit methods, however, requre large computer memory and the inversion of the block multidiagonal system of algebraic equations. These are difficult to implement to take advantage of the hardware of the vector-processing computers. An alternative is to evaluate the chemistry source terms in the species equations implicitly while other terms, not contributing to stiffness, are evaluated explicitly. This semi-implicit method was proposed by several investigators [28-31].

6

A stability analysis [31] reveals that by linearizing the implicit source terms one ends up with a preconditioning matrix which modifies the unsteady terms of the governing equations. The preconditioning matrix allows each species to evolve at its own characteristic time scale. With implicit source terms, the governing parameter is now the fluid dynamics time scale which, in turn, is dictated by the Courant-Friedrichs-Lewy (CFL) condition.

The partially implicit method and the global two-step chemistry model [18] was used successfully by Drummond, et al. [32] to calculate premixed H_2-air reacting flow using a spectral method. Bussing and Murman [31, 33] used a finite volume method to solve for flows over ramps and rearward facing steps. Chitsomboon and Tiwari [34] used a finite difference method for similar problems. Eklund et al. [27], studied relative merits of an Adams scheme and a Runge-Kutta scheme. A nonpremixed calculation of this particular type of reacting flow was done by Chitsomboon et al. [35]; in the study, gaseous hydrogen fuel was injected perpendicular to the sidewalls and the fuel struts of an inlet-combustor configuration. The results reported in these studies have indicated that the semi-implicit method together with the global two-step chemistry model provides a viable tool in numerical study of H_2-air reacting flow by using the elliptic governing equations.

As mentioned earlier, the flow field far downstream of the fuel injectors is relatively less complex; a predominant flow direction exists in which there is no flow separation. If only a steady state solution is sought, a class of approximation to the fully elliptic equations, parabolized approximation, is physically reasonable. The motivation in doing this kind of approximation is that an N-dimensional problem reduces to an (N-1)-dimensional problem. Furthermore, the reduced dimension problem can

be solved by marching in the flow direction once (or, at most, a couple of times) instead of marching in time for many steps as in the elliptic procedure. This method is highly efficient with regard to memory requirement and total CPU time of the computer program. A brief discussion of this particular approximation is given below.

The boundary layer approximation introduced by Prandtl at the turn of the century has enjoyed a wealth of analyses both analytically and numerically (see, e.g., Refs. 36-38 and references therein). An order of magnitude analysis shows that, for a high Reynolds number flow, the streamwise diffusion terms and the whole normal momentum equation can be dropped since they are terms of high order. The remaining steady state equations, with the streamwise pressure gradient specified, are mathematically parabolic and can be solved by integration in the streamwise direction provided appropriate initial and boundary conditions are supplied. In its original inception, the boundary layer equations were used to correct for thin viscous effects near solid walls of the outer inviscid solution. The streamwise pressure gradient can be obtained from the inviscid solution; this method has been termed the direct method. Due to the neglect of the normal momentum equation, the direct method cannot resolve the viscous-inviscid interaction which could be important for some classes of flow. To partially account for the interaction, modified methods such as the inverse method or the interacting boundary layer method must be used. Numerical algorithms of these methods could be quite tedious since they require adaptive adjustments of various parameters.

Parabolized approximation contains all the boundary layer equations plus the normal momentum equation. The inclusion of the normal momentum equation makes the equations very versatile. First of all, the entire Euler

equations are included; this eradicates the need of laborious patching of viscous and inviscid solutions required by the boundary layer procedure. The viscous-inviscid interactions in the normal direction are naturally represented and the equations still enjoy the efficient procedure of space marching in obtaining the solution. Like the boundary layer approximation, this approximation is valid for high Reynolds number flows only. Traditionally, the equations are termed "parabolic" if the streamwise pressure gradient is prescribed a priori. The equations are called "parabolized" if mathematical treatments are done to the pressure gradient term such that the term can be retained as part of the solution without causing any illposedness. Some investigators prefer to call both formulations as reduced Navier-Stokes equations (RNS).

It appears that Ferri [39] and Rudman and Rubin [40] are among the first to propose using this class of approximation to the full Navier-Stokes equations. Since then, it has found numerous applications from the incompressible regime to the hypersonic regime for both external and internal flow.

For imcompressible and subsonic flows, characteristics of downstream flow can affect those at upstream since the pressure waves which propagate disturbances in the flow travel faster than the local fluid velocity. For supersonic flow, information can still propagate upstream through subsonic boundary layers close to solid walls. In essence, a disturbance at a point in the domain affects the solution through out the domain; this constitutes an elliptic boundary value problem. If the untreated parabolized equations are marched with the pressure determined as part of the solution, then, the equations are illposed since they represent an elliptic boundary value problem with a parabolic initial value problem. The mathematical

9

characteristic of the equations is controlled by the streamwise pressure gradient term in the streamwise momentum equation. Lighthill [41] demonstrated the existence of an exponentially growing solution (called the departure solution) which reflects illposedness by retaining the streamwise pressure gradient term. Lubard and Helliwell [42] showed that for a backward difference on the streamwise pressure gradient term, the departure solution can be avoided if the integration step size (Δx) is greater than $(\overline{\Delta x})$ where $\overline{\Delta x}$ is of the order of magnitude of the subsonic layer thickness. This is a rather paradoxical conclusion since one would expect that the smaller the integration step size the more accurate and the more stable the solution will be. However, if Δx is less than $\overline{\Delta x}$ (which is the extent of upstream interaction) the parabolized equations will try to represent upstream influence and will result in a departure solution. If the pressure field can be prescribed a priori, however, the equations are mathematically parabolic and there is no difficulty in marching in the streamwise direction. The initial prescribed pressure field can be updated once the entire domain is swept. This is accomplished by a Poisson equation for pressure derived from the momentum equations. Schemes based on this procedure are quite expensive since the Poisson equation might have to be solved several times [43-45], but it is still relatively economical as compared to using the fully elliptic equations.

Algorithms which are valid from the incompressible regime to the hypersonic regime which do not require solution to the Poisson equation have been reported in [46-48]. These algorithms used forward difference on the pressure gradient term which necessitates a known or guessed pressure field. The departure behavior has been claimed to be taken care of by the forward difference procedure. Also, global iterations on the pressure field, by

multiple sweeping of the domain, become necessary in order to correct the guessed pressure field. Another widely used algorithm was developed by Patankar and Spalding [49]. This is a single sweep method for incompressible flow. The assumed pressure field and the velocity field are corrected simultaneously once an integration step is completed. The correction is made in a manner such that the continuity equation, which is not included in the implicit solution procedure, is satisfied. An extension of the algorithm to compressible flows was made in [50]. The modified algorithm does not seem to capture shock wave well due probably to the nature of the pressure correction procedure [51]. Global iteration on the pressure field was also studied [52]; it was found that the iteration had quite an effect on the characteristic of the flow field.

For supersonic high Reynolds number flow without streamwise separation, the algorithm of Vigneron et al. [53] is very efficient and accurate. The accuracy is partially attained by solving all the governing equations in a fully coupled manner. The algorithm is really a steady state version of those proposed by Beam and Warming [54] and Briley and McDonald [55]. Since it is a non-iterative single sweep method, the algorithm is very efficient. The only cumbersome part of the method is that one has to evaluate the Jacobian matrices of all the flux vectors and solve them in a block tri-diagonal manner instead of just a scalar tri-diagonal procedure encountered in the previously discussed methods. The departure behavior of the solution is suppressed by retaining only a fraction, ω, of the streamwise pressure gradient within the subsonic portions of a boundary layer. The parameter, ω, was obtained from an eigenvalue analysis of the locally linearized governing equations such that the equations become wellposed. By just manipulating the governing equations, Khosla and Lai [56] have also revealed the

11

existence of the parameter ω. A similar fully coupled fully implicit algorithm was developed also by Schiff and Steger [57]. An elaborate eigenvalue analysis revealed again that the ill-posedness of the system of equations is caused by the streamwise pressure gradient in the subsonic layer. To render the equations well posed, a sublayer approximation was then proposed. In this approximation, the pressure gradient within the subsonic zone close to a solid wall is evaluated at the first supersonic mesh point away from the wall. In an independent study, the sublayer model was also proposed by Rubin and Lin [58].

Another good feature of this type of algorithm is that it can be cast into a fully conservative form, thus, capable of capturing strong shock waves. Rakich [59] and Chitsomboon et al. [9] applied global iteration procedures on the pressure field to this algorithm for attached and separated flows, respectively. A modified form of the FLARE approximation [60] was used in solving flows with streamwise separations.

Parabolic governing equations are quite popular in solving supersonic chemically reacting flows of hydrogen and air [50, 52, 61-62]. The algorithm used in these studies is that of Partankar and Spalding [49] with a compressibility correction for the pressure-velocity update procedure. Equilibrium chemistry models were used in all of these studies. Finite-rate chemistry models were employed by Rogers and Chinitz [18] for solving similar flows in which gaseous hydrogen is injected parallel to the flow direction. Some difficulties were reported in using a finite-rate chemistry model. Some of the species concentrations became negative and the computer program could not continue but there was no discussion as to how the chemistry source terms were evaluated [18]. A finite rate chemistry model was also utilized by Sinha and Dash [63]. In their study, the species equations

were decoupled from the fluid dynamics equations and the chemistry source terms for the next integration step were obtained by a shooting technique. As discussed earlier, the Patankar-Spalding-based algorithm probably could not capture strong shock waves typical of flow in a scramjet; thus limiting the application of the algorithm to relatively simple flows. For flows with embedded strong shock waves, particularly those with strong interactions between chemistry and fluid, an alternative approach is warranted.

1.3 Objectives

The objectives of this study are to, first, incorporate the finite-rate chemistry package of Rogers and Chinitz [18] into an existing nonreacting elliptic computer code. This code was developed initially for solving flows in inlets of scramjet engine configurations [5, 64]. The unsplit MacCormack finite difference algorithm was used to advance the discretized form of the two-dimensional Navier-Stokes equations in time until a steady state solution is attained. The code is fully vectorized and is operational only on the VPS-32 vector processing computer at the NASA-LaRC (an upgraded version of the CDC Cyber-205). The incorporation of the chemistry package has included four species continuity equations along with the original set of the governing equations. The energy equation is also modified to make it appropriate for a chemically reacting flow. Stiffness associated with fast chemical reactions is alleviated by evaluating the chemistry source terms implicitly. The resulting computer code will be used to solve various reacting H_2-air problems related to scramjet engine configurations.

A second computer code, based on fully implicit parabolized methods of Vigneron et al. [53] and Schiff and Steger [57], is also developed. The reason for using this particular algorithm is to capture strong shock waves

typical of the flow problems for which the code is developed. The thermo-chemical models employed here are the same as those used in the fully elliptic procedure. The chemistry equations and the fluid dynamics equations are solved in a fully implicit fully coupled manner in order to resolve the fluid-chemistry interactions. The results obtained by using this space marching code will be compared with those obtained by using the more expensive elliptic code.

The basic formulations for this study are described in Section 2. The eliptic and the parabolized governing equations are presented together with the thermo-chemical models and other important formulations. The finite difference algorithms for both the elliptic and the parabolized equations are presented in Section 3 where other related informations are also provided. The important results obtained in this study are presented and discussed in Section 4. Finally, specific conclusions and some suggestions for further study are provided in Section 5.

2. BASIC FORMULATION

This section deals with the discussion of the physical model and basic governing equations for the elliptic and parabolized formulations. The relations for the chemistry and thermodynamic models are also provided.

2.1 Physical Model

As pointed out in the introduction, the primary goal of this study is to compute chemically reacting flow through the scramjet engine. A schematic of a scramjet engine is shown in Fig. 2.1 in which it is shown that the engine consists of many identical modules; the size of a module is appropriate for ground testing. An engine module and a part of its topview are also illustrated. The fuel is injected from the fuel struts as

FUEL INJECTION STRUTS

COMBUSTOR

NOZZLE

COWL

INLET

CROSS SECTION OF STRUT REGION
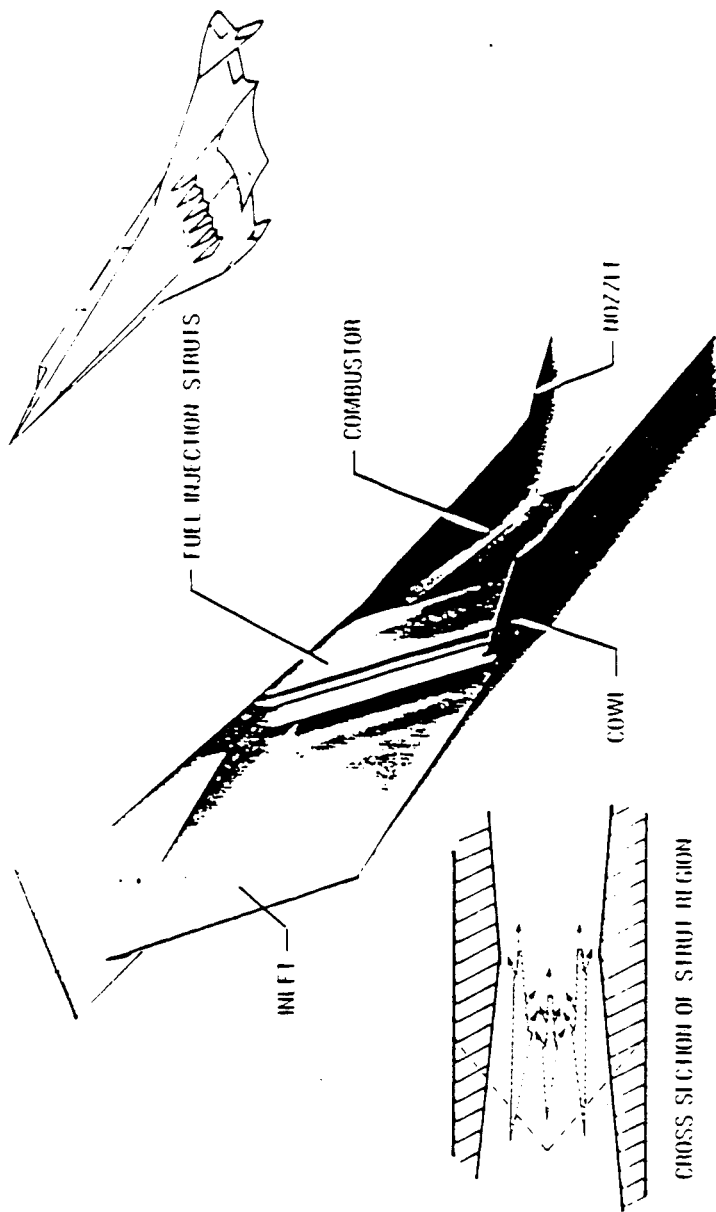
Fig. **2.**1 Scramjet engine module and its cross section.

indicated by the arrows. Figure 2.2 depicts the complex flow field in the vicinity of a fuel injector. To resolve the complexity of the flow in the near field of the injector, the fully elliptic form of the governing equations must be used. The parabolized form of the governing equations as discussed in the introduction can be used in the region far downstream of the fuel injector in which the flow becomes less complex.

2.2 Elliptic Governing Equations

The two-dimensional Navier-Stokes equations and the species continuity equations in body-fitted coordinate system written in the strong conversation law form can be expressed symbolically as

$$\frac{\partial q}{\partial t} + \frac{\partial E}{\partial \xi} + \frac{\partial F}{\partial \eta} = \frac{W}{J} \tag{2.1}$$

where

$$q = \frac{1}{J} \left[\rho, \ \rho u, \ \rho v, \ \rho H - p, \ \rho_i \right]^T \tag{2.2}$$

$$E = \begin{bmatrix} \overline{\rho u} \\ \rho \overline{uu} + y_\eta \tau_{xx} - x_\eta \tau_{xy} \\ \rho \overline{vu} + y_\eta \tau_{yx} - x_\eta \tau_{yy} \\ (\rho H - p)\overline{u} + y_\eta (u\tau_{xx} + v\tau_{xy} + q_x) - x_\eta (v\tau_{yy} + u\tau_{yx} + q_y) \\ \rho_i \overline{u} + y_\eta (\beta (f_i)_x) - x_\eta (\beta (f_i)_y) \end{bmatrix} \tag{2.3}$$

16

MIXING BOUNDARY

JET SHOCKS

MACH DISC

REATTACHMENT

BOW SHOCK

FUEL

SEPARATION

M_∞
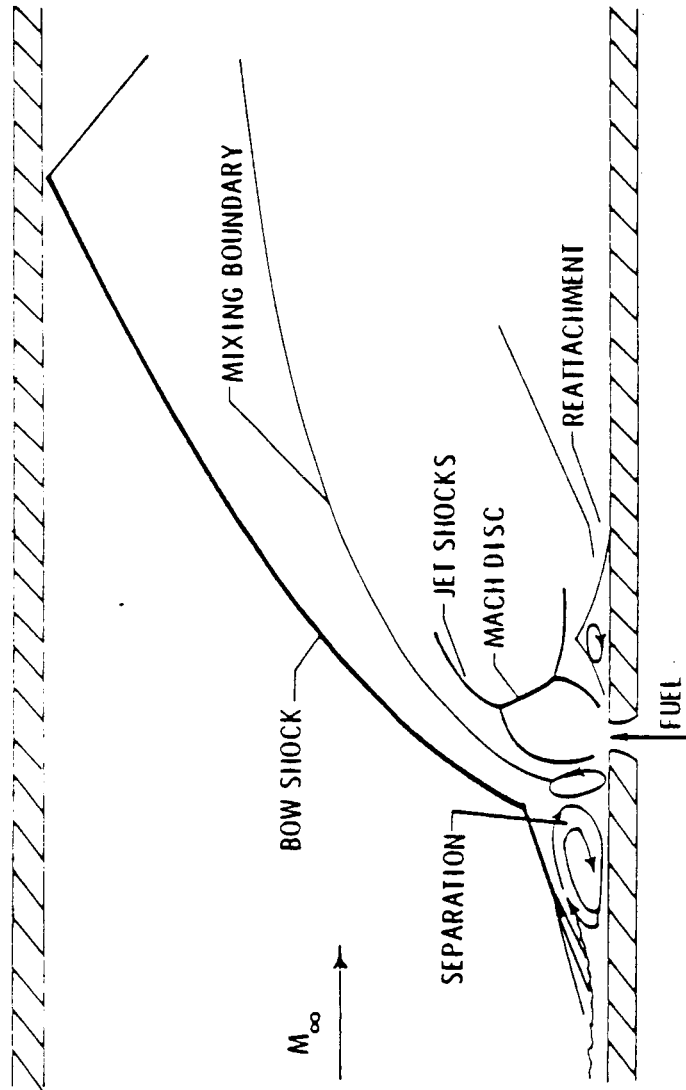
Fig. 2.2 Flow field near an injector.

17

$$
F = \begin{bmatrix}
\rho\overline{V} \\[6pt]
\rho\overline{u}V - y_\xi \tau_{xx} + x_\xi \tau_{xy} \\[6pt]
\rho\overline{v}u - y_\xi \tau_{yx} + x_\xi \tau_{yy} \\[6pt]
(\rho H - p)\overline{V} - y_\xi(u\tau_{xx} + v\tau_{xy} + q_x) + x_\xi(u\tau_{yx} + v\tau_{yy} + q_y) \\[6pt]
\rho_i \overline{V} - y_\xi(\beta(f_i)_x) + x_\xi(\beta(f_i)_y)
\end{bmatrix} . \tag{2.4}
$$

Here, x_ξ denotes $\partial x/\partial \xi$, and so forth, and

$$
\overline{u} = y_\eta u - x_\eta v \tag{2.5a}
$$

$$
\overline{v} = -y_\xi u + x_\xi v \tag{2.5b}
$$

$$
J = (x_\xi y_\eta - x_\eta y_\xi)^{-1}. \tag{2.5c}
$$

It is to be understood that the source terms, W, for the Navier-Stokes equations are identically zero. For the species equations in source terms represent rates of species production or extinction to be discussed in detail in the subsequent section. The quantities τ_{xx}, τ_{xy}, and τ_{yy} are components of the stress tensor. With the Stokes hypothesis assumed, these quantities are given by

$$
\tau_{xx} = p - (\mu + \mu_t)\left(\frac{4}{3}\frac{\partial u}{\partial x} - \frac{2}{3}\frac{\partial v}{\partial y}\right) \tag{2.6a}
$$

$$
\tau_{xy} = \tau_{yx} = -(\mu + \mu_t)\left(\frac{\partial u}{\partial y} + \frac{\partial v}{\partial x}\right) \tag{2.6b}
$$

$$
\tau_{yy} = p + (\mu + \mu_t)\left(\frac{2}{3}\frac{\partial u}{\partial x} - \frac{4}{3}\frac{\partial v}{\partial y}\right). \tag{2.6c}
$$

The quantities q_x and q_y are components of the heat flux; the fluxes are due

18

to heat conduction and transport of enthalpy by species diffusion. For a laminar flow the terms are given by

$$q_x = - k \frac{\partial T}{\partial x} - \rho D \sum_{i=1}^{N} [(\frac{\partial f_i}{\partial x}) h_i] \qquad (2.7a)$$

$$q_y = - k \frac{\partial T}{\partial y} - \rho D \sum_{i=1}^{N} [(\frac{\partial f_i}{\partial y}) h_i] \qquad (2.7b)$$

where

$$h_i = H_i^0 + \int_0^T C_{pi} \, dT \, . \qquad (2.8)$$

Note that the effective binary diffusion coefficient, D, is used for all species. Together with the assumption that the Lewis number is unity, the approximation provides a great simplification to these heat fluxes. The assumption, while not always stated explicitly, appears to be a fairly routine assumption in the analysis of gas phase reacting systems. With the manipulation presented in Appendix A, the heat flux terms can be written simply as

$$q_x = - (\frac{\mu}{Pr}) \frac{\partial h}{\partial x} \qquad (2.9a)$$

$$q_y = - (\frac{\mu}{Pr}) \frac{\partial h}{\partial y} \, . \qquad (2.9b)$$

For a turbulent flow the terms are modified as

$$q_x = - \left(\frac{\mu}{Pr} + \frac{\mu_t}{Pr_t}\right) \frac{\partial h}{\partial x} \tag{2.10a}$$

$$q_y = - \left(\frac{\mu}{Pr} + \frac{\mu_t}{Pr_t}\right) \frac{\partial h}{\partial y} \; . \tag{2.10b}$$

The molecular viscosity, μ, is assumed to be dependent upon temperature and is calculated by the Sutherland's formula:

$$\mu = \frac{(1.458 \times 10^{-6}) \; T^{3/2}}{T + 110.4} \; . \tag{2.11}$$

Pure air properties are used in the above relation since the mixture is dominated by the nitrogen species. The turbulence eddy viscosity, μ_t, is obtained by the algebraic two-layer eddy viscosity model of Baldwin and Lomax [65]. In this model, the inner layer is represented by the Prandtl-Van Driest mixing length formulation and the Clauser approximation is used in the outer layer. The model is very convenient to use since there is no need to find the edge of a boundary layer like some other algebraic models. The study of Peters et al. [66] shows that it is a viable turbulence model and provides a good starting point in turbulence modeling. The laminar and turbulent Prandtl numbers are assumed to be equal to constant values of 0.72 and 0.9, respectively.

The subscript i's in the species equations range from one to four and denote the species O_2, H_2O, H_2 and OH, respectively. The mass fraction of nigroten can be obtained by the mass constraint relation:

$$f_5 = 1 - \sum_{i=1}^{4} f_i . \qquad (2.12)$$

The quantity β in the species diffusion terms is defined as

$$\beta = - \left(\frac{\mu}{Le \cdot Pr} + \frac{\mu_t}{Le_t \cdot Pr_t} \right) \qquad (2.13)$$

where

$$Le = \alpha/D = 1 \qquad (2.14)$$

and

$$Pr = \nu/\alpha . \qquad (2.15)$$

The laminar and turbulent Lewis numbers are assumed to be equal to one.

2.3 Parabolized Governing Equations

The two-dimensional parabolized Navier-Stokes and parabolized species equations in a body-fitted coordinate system are expressed in a strong conservation law form as

$$\frac{\partial E}{\partial \xi} + \frac{\partial \overline{P}}{\partial \xi} + \frac{\partial (F_i + F_v)}{\partial \eta} = \frac{W_i}{J} \qquad (2.16)$$

where

$$\overline{P} = \frac{1}{J} \left[0, \ \xi_x (1-\omega)p, \ \xi_y (1-\omega)p, \ 0, \ 0, \ 0, \ 0, \ 0 \right]^T \qquad (2.17)$$

21

$$E = \frac{\xi_x}{J} \begin{bmatrix} \rho u \\ \rho uu + \omega p \\ \rho uv \\ \rho Hu \\ \rho_i u \end{bmatrix} + \frac{\xi_y}{J} \begin{bmatrix} \rho v \\ \rho uv \\ \rho vv + \omega p \\ \rho Hv \\ \rho_i v \end{bmatrix} \qquad (2.18)$$

$$F_i = \frac{\eta_x}{J} \begin{bmatrix} \rho u \\ \rho uu + p \\ \rho uv \\ \rho Hu \\ \rho_i u \end{bmatrix} + \frac{\eta_y}{J} \begin{bmatrix} \rho v \\ \rho uv \\ \rho vv + p \\ \rho Hv \\ \rho_i v \end{bmatrix} \qquad (2.19)$$

$$F_v = \frac{\eta_x}{J} \begin{bmatrix} 0 \\ \tau_{xx} \\ \tau_{xy} \\ u\tau_{xx} + v\tau_{xy} + q_x \\ (\beta f_i)_x \end{bmatrix} + \frac{\eta_y}{J} \begin{bmatrix} 0 \\ \tau_{yx} \\ \tau_{yy} \\ u\tau_{yx} + v\tau_{yy} + q_y \\ (\beta f_i)_y \end{bmatrix} . \qquad (2.20)$$

The derivatives in the viscous flux, F, are given as

$$\tau_{xx} = -(\mu + \mu_t)(\frac{4}{3}\eta_x u_\eta - \frac{2}{3}\eta_y v_\eta) \qquad (2.21a)$$

$$\tau_{xy} = -(\mu + \mu_t)(\eta_y u_\eta + \eta_x v_\eta) \qquad (2.21b)$$

$$\tau_{yy} = -(\mu + \mu_t)(\frac{4}{3}\eta_y v_\eta - \frac{2}{3}\eta_x u_\eta) \qquad (2.21c)$$

$$q_x = - (\frac{\mu}{Pr} + \frac{\mu_t}{Pr_t}) \, n_x \, h_n \qquad \qquad (2.22a)$$

$$q_y = - (\frac{\mu}{Pr} + \frac{\mu_t}{Pr_t}) \, n_y \, h_n \qquad \qquad (2.22b)$$

$$(\beta f_i)_x = n_x (\beta f_i)_n \qquad \qquad (2.23a)$$

$$(\beta f_i)_y = n_y (\beta f_i)_n \, . \qquad \qquad (2.23b)$$

The above parabolized equations are obtained by dropping the unsteady terms and the streamwise viscous derivative terms. For high Reynolds number flows, neglect of these terms should not degrade quality of the solution by much since they are high order terms. Note also that only a fraction ω of the streamwise pressure gradients are retained. The parameter ω is a quantity of magnitude varying between zero and one and is obtained from an eigenvalue analysis [53]. The relation for ω is given in terms of the streamwise Mach number as

$$\omega = \frac{\gamma M_x^2}{1+(\gamma-1)M_x^2} \, . \qquad \qquad (2.24)$$

From the above relation, it can be seen that ω is equal to zero when the streamwise Mach number, M_x, equals zero; it is equal to unity when M_x equals one. For M_x greater than one, i.e., supersonic flow, ω is assigned the value of one. The parameter ω is necessary in order to suppress upstream pressure interactions. From a mathematical viewpoint, ω suppresses the
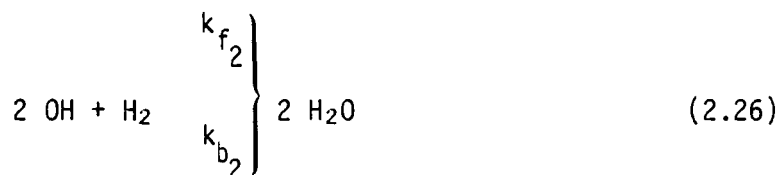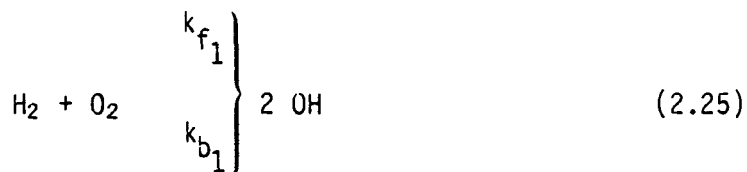
ellipticity of the equations rendering them well posed for marching in the ξ direction. It is natural to expect that this technique will work well only for supersonic high Reynolds number flows where subsonic layers close to solid walls are thin. For flows with large subsonic zones, alternative methods, such as those discussed in the introduction, are recommended.

In the supersonic region, the full Euler equations are included; the equations should have capability to capture strong shock waves. The normal pressure gradient is also retained in full; this allows free pressure interaction in the cross stream direction without having to resort to the explicit interaction mechanism used in boundary-layer techniques.

The quantities μ, Pr and β are obtained in the same manner as those for the elliptic equations. The vorticity which is required in the algebraic turbulence model is evaluated by retaining only the cross stream component.

2.4 Chemistry Model

A chemistry model is needed in order to obtain the chemistry source terms, W, as functions of the dependent variables, q. In this study, the global two-step finite-rate chemistry model of Rogers and Chinitz [18] is adopted. The model is given by

$$H_2 + O_2 \overset{k_{f_1}}{\underset{k_{b_1}}{\rightleftharpoons}} 2\ OH \tag{2.25}$$

$$2\ OH + H_2 \overset{k_{f_2}}{\underset{k_{b_2}}{\rightleftharpoons}} 2\ H_2O \tag{2.26}$$

where the k_f's are the forward reaction rate constants and the k_b's are the

backward reaction rate constants. The chemistry source terms can be obtained by applying the law of mass action to the two reaction equations. For a general reaction equation:

$$\sum_{j=1}^{J} A_{ij} C_j \quad \substack{k_{f_i} \\ \overrightarrow{} \\ \overleftarrow{} \\ k_{b_i}} \quad \sum_{j=1}^{J} B_{ij} C_j \; ; \quad i=1,2,\ldots,I \qquad (2.27)$$

the law of mass action states that the rate of change of molar concentration of the (j)th species by the (i)th reaction is given by

$$(C_j')_i = (B_{ij} - A_{ij}) \left[k_{fi} \prod_{k=1}^{J} C_k^{A_{ik}} - k_{bi} \prod_{k=1}^{J} C_k^{B_{ik}} \right]. \qquad (2.28)$$

The total rate of change in molar concentration of the (j)th species is obtained by summing over all the reaction equations

$$C_j' = \sum_{i=1}^{I} (C_j')_i \qquad (2.29)$$

The source terms on mass basis, W, are finally found by multiplying the molar changes by the corresponding molecular weights

$$W_j = C_j' M_j. \qquad (2.30)$$

By applying the law of mass action to the present two-step global model, the chemistry source terms on the mass basis are given as

$$W_1 = -\frac{k_{f1}\, \rho_1\, \rho_3}{M_3} + \frac{k_{b1}\, M_1\, \rho_4^2}{M_4^2} \qquad (2.31a)$$

$$W_2 = \frac{2\, k_{f2}\, M_2\, \rho_3\, \rho_4^2}{M_3 M_4^2} - \frac{2\, k_{b2}\, \rho_2^2}{M_2} \qquad (2.31b)$$

$$W_3 = \frac{M_3\, W_1}{M_1} - \frac{M_3\, W_2}{2M_2} \qquad (2.31c)$$

$$W_4 = -\frac{2\, M_4\, W_1}{M_1} - \frac{M_4 W_2}{M_2} \qquad (2.31d)$$

where subscripts 1,2,3, and 4 are used to represent O_2, H_2O, H_2, and OH, respectively.

The forward reaction rates are computed from the Arrhenius' law

$$k_{fi} = A_i\, T^{N_i}\, e^{-E_i/R^0 T}. \qquad (2.32a)$$

For the present model the rates are given by

$$K_{f1} = A_1\, T^{-10}\, e^{-4865/R^0 T} \qquad (2.32b)$$

$$k_{f2} = A_2\, T^{-13}\, e^{-42500/R^0 T} \qquad (2.32c)$$

where

$$A_1 = (8.9170 + 31.433/\emptyset - 28.95)(10)^{44} \quad m^3/kmol\text{-}sec. \qquad (2.33a)$$

$$A_2 = (2 + 1.333/\phi - 0.833\phi)(10)^{58} \qquad m^6/kmol^2\text{-sec.} \qquad (2.33b)$$

$$R^0 = 1.1972 \quad cal/mole\text{-}K. \qquad (2.34)$$

Note that the pre-exponential constants, A_i, are dependent upon equivalence ratio, ϕ; the functions were determined by curve fitting such that the rates agree well with the more sophisticated model [18]. The backward rate constants are related to the forward rate constants by

$$k_{bi} = k_{fi}/K_i \qquad (2.35)$$

where K_i's are equilibrium constants. The values for K_i's are given by

$$K_1 = 26.16 \, e^{-8992/T} \qquad (2.36a)$$

$$K_2 = (2.682 \times 10^{-9})(T) \, e^{69415/T} \qquad m^3/kmol. \qquad (2.36b)$$

It should be noted here that the global two-step chemistry model is not accurate for predicting flames with long ignition delay times for temperature on the order of 1000 K. Specifically, the reaction would proceed continuously without a delay period even if the mixture temperature is below the ignition temperature. To prevent this nonphysical phenomenon, a cut off temperature of 1000 K was used to control the reaction, i.e., if temperature of the mixture is less than 1000 K, reaction is not permitted.

The model is used unmodified for the parabolized formulation.

2.5 Thermodynamics Model

In general, thermodynamic properties of the mixture are computed by summing properties of individual species weighted by species mass fractions. The specific heat at constant pressure of the (i)th species is assumed to be a linear function of temperature

$$C_{pi} = a_i + b_i T \qquad (2.37)$$

where a_i and b_i are constants which are obtained by curve fitting the thermochemical data of Ref. 67. The numerical values of these constants are given in Table 2.1. The static enthalpy of the mixture can be expressed as

$$h = \sum_{i=1}^{5} f_i H_i + \overline{C}_p T \qquad (2.38)$$

where

$$\overline{C}_p = \sum_{i=1}^{5} f_i (a_i + 0.5 b_i T) . \qquad (2.39)$$

The total enthalpy can now be given by

$$H = h + 0.5 (u^2 + v^2) . \qquad (2.40)$$

The mixture gas constant can be obtained by a mass weighted summation over all species as

$$\overline{R} = \sum_{i=1}^{5} f_i R_i . \qquad (2.41)$$

Table 2.1 Numerical values of various constants

Species	$H°$(Joule/kg)	a	b	R(Joule/kg-K)
O_2	-271,267	0.1198	947	254
H_2O	-13,972,530	0.4391	1858	457
H_2	-4,200,188	2.0546	12867	4035
OH	+1,772,591	0.1656	1673	478
N_2	-309,483	0.1035	1048	240

The equation of state for the mixture can be written as

$$p = \rho \bar{R} T \qquad (2.42)$$

Finally, the specific heat ratio of the mixture is calculated from

$$\gamma = \frac{\bar{C}_p}{\bar{C}_p - \bar{R}} \qquad (2.43)$$

3. METHODS OF SOLUTION

In this section the finite difference algorithms for the elliptic and the parabolized formulations are presented. Also discussed are the boundary conditions and the smoothing functions used in both formulations. The grid generation technique is given in section 3.5. Some important procedures in obtaining solutions are finally described in section 3.6.

3.1 Algorithm for Elliptic Equations

The symbolic form of the elliptic equations in body-fitted coordinate is written here again as

$$\frac{\partial q}{\partial t} = - \left(\frac{\partial E}{\partial \xi} + \frac{\partial F}{\partial \eta} - Q \right) \qquad (3.1)$$

where $Q = W/J$ for the species equations. Equation (3.1) can be forward differenced in time as

$$q^{n+1} - q^n = -\Delta t \left(\frac{\partial E^n}{\partial \xi} + \frac{\partial F^n}{\partial \eta} - Q^{n+1}\right) \qquad (3.2)$$

where (n+1) denotes the time level where solution is being sought. Note that the source terms, Q, are evaluated at the implicit time level (n+1) to alleviate stiffness associated with fast chemical reactions as discussed earlier. Since the source terms are nonlinear functions of the dependent variable vector, they must be linearized to render linear discrete equations for solution. By using the Newton linearization scheme, one obtains

$$Q^{n+1} = Q^n + \left(\frac{\partial Q}{\partial q}\right)^n (q^{n+1} - q^n) . \qquad (3.3)$$

The dependent variables, q, in the above equation are the ρ_i/J of the four species. Since both Q and q are vectors of four elements, the term $\partial Q/\partial q$ becomes a 4x4 Jacobian matrix. Upon defining:

$$M = \partial Q/\partial q \qquad (3.4)$$

$$\Delta q^n = q^{n+1} - q^n \qquad (3.5)$$

$$R = \frac{\partial E}{\partial \xi} + \frac{\partial F}{\partial \eta} - Q \qquad (3.6)$$

and substituting Eqs. (3.3-3.6) into Eq. (3.2) one obtains

$$(I - \Delta t \, M)^n \, \Delta q^n = -\Delta t(R^n) \qquad (3.7)$$

31

where I is the identity matrix. Equation (3.7) yields explicit relations for the Navier-Stokes part whereas the species continuity equations give rise to a block mono-diagonal system of algebraic equations. Components of the Jacobian matrix, M, are given in Appendix B. The unsplit MacCormack algorithm [68] can now be applied to Eq. (3.7) as follows:

Predictor step:

$$(I - \Delta t \ M)^n \overline{\Delta q^n} = - \Delta t \ R_f^n \tag{3.8a}$$

$$\overline{q^{n+1}} = q^n + \overline{\Delta q^n} \tag{3.8b}$$

Corrector step:

$$(I - \Delta t \ M)^{\overline{n+1}} \Delta q^n = - \Delta t \ R_b^{\overline{n+1}} \tag{3.9a}$$

$$q^{n+1} = q^n + 0.5(\overline{\Delta q^n} + \Delta q^n). \tag{3.9b}$$

The subscripts f and b in Eqs. (3.8a) and (3.9a) denote forward and backward finite difference, respectively.

3.2 Algorithm for Parabolized Equations

For convenience, the symbolic form of the parabolized equations in body-fitted coordinates are expressed here again as

$$\frac{\partial E}{\partial \xi} + \frac{\partial \overline{P}}{\partial \xi} + \frac{\partial}{\partial \eta} (F_I + F_v) = Q. \tag{3.10}$$

The Beam and Warming finite difference algorithm [54] is used to discretize Eq. (3.10). The algorithm was initially proposed for time dependent equations; the modifications for the present steady state equations are obvious upon replacing the marching direction with ξ coordinate. The algorithm for Eq. (3.10) can then be written as

$$\Delta^n E + \frac{(\Delta\xi)a}{1 + b} \left[\frac{\partial}{\partial\eta} \Delta^n (F_I + F_v) - \Delta^n Q \right]$$

$$= - \Delta\xi \left[\frac{\partial}{\partial\eta} (F_I + F_v) - Q \right]^n + \frac{b}{1 + b} \Delta^{n-1} E$$

$$- \frac{\partial \overline{P}}{\partial\xi} + 0 \, (a - b - 0.5)(\Delta\xi)^2 + 0(\Delta\xi)^3. \tag{3.11}$$

Many numerical schemes can be generated by varying the two parameters, a and b. Some familiar schemes are given below:

    a = 0 , b = 0   ; Euler explicit

    a = 1 , b = 0   ; Euler implicit

    a = 1 , b = 0.5 ; Three-point backward

    a = 0.5, b = 0   ; Trapezoidal

If the difference between a and b is equal to one half, the algorithm is second order accurate in the ξ direction, otherwise it is first order accurate.

Since the flux terms and the chemistry source terms are all nonlinear functions of the dependent variable vector and the metric quantities of coordinate transformation, they need to be linearized. Unless an appropri-

ate linearization scheme is adopted, the conservative property of the algorithm given in Eq. (3.11) will be disrupted. Conservative linearization is very important particularly for internal flow where mass flow rate across the channel has to remain constant. Also, shock waves will not be captured accurately if the linearization procedure disturbs the conservative property of the algorithm. Another important consideration is that the linearization scheme should honor the formal accuracy of the algorithm. In this study, a scheme very similar to that used by Schiff and Steger [57] is used to linearize the nonlinear terms. The general technique is to express the terms to be linearized as functions of the dependent variable vector, q, and the metric quantities; only the terms involving q are linearized, the metrics are frozen at the implicit level. This is nothing but a basic mathematical operation for a function of multiple variables. The nonlinear terms are linearized as follows:

$$\Delta^n E = E^{n+1} - E^n = [\tilde{E}^n + (\frac{\partial \tilde{E}}{\partial q})^n \Delta^n q] - [\tilde{E}^{n-1} + (\frac{\partial \tilde{E}}{\partial q})^{n-1} \Delta^{n-1} q] + O(\Delta \xi)^3 \quad (3.12)$$

$$\Delta^n F_{I,v} = (\frac{\partial \tilde{F}}{\partial q} I,v)^n \Delta^n q + O(\Delta \xi)^2 \quad (3.13)$$

$$\Delta^n Q = (\frac{\partial \tilde{Q}}{\partial q})^n \Delta^n q + O(\Delta \xi)^2 \quad (3.14)$$

where a tilde over a quantity means that quantity is to be evaluated by using q at the indicated level whereas the metric quantities are evaluated at the indicated level plus one. Note that the (n+1) and the (n) terms of

the streamwise flux, E, are linearized in the same fashion to ensure the conservative property in the ξ direction; it is also second order accurate. Even if a first order accurate algorithm in the ξ direction is desired one must still linearize in this manner to ensure a conservative scheme. The cross stream flux, however, is linearized nonconservatively in ξ direction since it is already represented in a divergence form in the η direction. The first order accuracy in linearization of F and Q is made second order accurate since the terms have $\Delta\xi$ in multiplication. The chemistry source terms are also linearized nonconservatively since they are non-conservative source terms in the first place. For convenience in algebraic manipulations, the following definitions are adopted:

$$\frac{\partial\overline{E}}{\partial q} = A \qquad (3.15)$$

$$\frac{\partial\widetilde{F}_{I,V}}{\partial q} = B_{I,V} \qquad (3.16)$$

$$\frac{\partial\widetilde{Q}}{\partial q} = C. \qquad (3.17)$$

Substituting Eqs. (3.12-3.17) into the original algorithm, Eq. (3.11), and rearranging one obtains

$$\left[A + \frac{\Delta\xi\, a}{1+b}\left\{\frac{\partial}{\partial\eta}\left(B_I + B_V\right) - C\right\}\right]^n \Delta^n q = - \Delta^{n-1}\tilde{E}$$

$$+ A^{n-1}\Delta^{n-1}q - \frac{\Delta\xi}{1+b}\left[\frac{\partial}{\partial\eta}\left(F_I + F_V\right) - Q\right]^n + \frac{b}{1+b}\Delta^{n-1}E$$

$$- \frac{\partial\overline{P}}{\partial\xi} + 0\,(a-b-0.5)(\Delta\xi)^2 + 0(\Delta\xi)^3. \tag{3.18}$$

The quantity in the brackets on the left-hand side of the above algorithm is an operator that applies on Δq^n rather than a multiplication per se. It is appropriate to note here that the dependent variable vector, q, in the present formulation is not the same one as used in the elliptic formulation. The intrinsic variable for the energy equation is selected as T/J rather than $(\rho H-p)/J$. The choice of this variable is quite arbitrary. The selection was made because it permits easy evaluation of the Jacobian matrices; it also gives a good diagonal dominance property for the momentum and the energy equations. As a matter of fact, many choices of dependent variable vectors were studied. They included:

$$q = [\rho,\ u,\ v,\ T,\ \rho_i]^T \tag{3.19}$$

$$q = [\rho,\ \rho u,\ \rho v,\ \rho H,\ \rho_i]^T/J \tag{3.20}$$

$$q = [\rho,\ \rho u,\ \rho v,\ \rho T,\ \rho_i]^T/J \tag{3.21}$$

$$q = [\rho,\ \rho u,\ \rho v,\ T,\ \rho_i]^T/J. \tag{3.22}$$

It was found that the last choice, Eq. (3.22), gave the best results. For

nonreacting flow, it has been traditional to use

$$q = [\rho, \rho u, \rho v, \rho e_t]^T / J \tag{3.23}$$

as the dependent variable vector [9, 53, 57]. The use of these variables, however, is not convenient for reacting flows since the pressure is related to other variables in a complicated way.

The linearized algorithm given in Eq. (3.18) yields a block tri-diagonal system of algebraic equations; the blocks are 8x8 matrices. By selecting the order of the dependent variables as in Eq. (3.22), the diagonal term of the Jacobian matrix, A, for the continuity equation is always equal to zero. Experiences with nonreacting flow studied in the past [8, 9] have indicated that the algorithm is not very robust; some kinds of implicit smoothing functions and/or stabilizing functions are always needed to prevent a division by zero during the inversion of the block tri-diagonal matrices. In this study, a method is proposed to improve robustness of the algorithm. In this method, the streamwise velocity in the continuity equation is partially lagged one step behind the implicit level where solution is being sought. To illustrate the point, the streamwise flux in delta form neglecting the metric quantities is given as

$$\Delta^n E = (\rho u)^{n+1} - (\rho u)^n . \tag{3.24}$$

The flux is then partially lagged as follows:

$$\Delta^n E = C_c u^n \rho^{n+1} + (1-C_c)(\rho u)^{n+1} - C_c u^{n-1} \rho^n - (1-C_c)(\rho u)^n \tag{3.25}$$

where C_c is a parameter of magnitude less than one. This modification renders the diagonal term of the continuity equation to be $C_c u^n$ rather than zero. Although the species continuity equations do not yield zero diagonal terms, their streamwise velocity is partially lagged in the same way as the continuity equation to ensure compatibility. For a second-order accurate scheme, the lagging procedure causes the continuity and the species equations to be somewhere between first and second order accurate depending on the magnitude of C_c. The conservative property, however, is not disturbed since the terms at (n+1) and at (n) are lagged in the same manner.

Some difficulties arise in evaluating the Jacobian matrix of the viscous flux. A typical component of the viscous flux is given as

$$\frac{\partial F_v}{\partial \eta} = \frac{\partial}{\partial \eta} \; \alpha_j \frac{\partial}{\partial \eta} \; f_j \tag{3.26}$$

where α is a function of the transport properties and metric quantities and f is a funtion of q. It is linearized and finite differenced as follows:

$$\frac{\partial}{\partial \eta} \frac{\partial F_v}{\partial q} = \frac{(\alpha_{j+1} + \alpha_j)}{2\Delta\eta} \frac{\left[(\partial f/\partial q)_{j+1} - (\partial f/\partial q)_j\right]}{\Delta\eta}$$

$$- \frac{(\alpha_j + \alpha_{j-1})}{2\Delta\eta} \frac{\left[(\partial f/\partial q)_j - (\partial f/\partial q)_{j-1}\right]}{\Delta\eta}. \tag{3.27}$$

This can be manipulated further to give a familiar-looking central difference scheme for a second order derivative.

If the flow to be investigated is of high Reynolds number and largely supersonic, a single sweep method will, in general, yield a very good solution. In this method, one has to march through the domain in the ξ direction only once. The term $\partial \bar{P}/\partial \xi$ can be included by lagging it one step behind the step where the solution is being sought; this could result in a departure solution since the elliptic effect is introduced for all practical purposes. For a departure-free solution the term $\partial \bar{P}/\partial \xi$ should be dropped [53]. The accuracy loss in neglecting this term should not be severe due to the thinness of the subsonic boundary layer. Reasonable results for non-reacting internal flow, using this method, were reported by Chitsomboon and Tiwari [8]. For flows with large subsonic pockets and/or streamwise separations, however, a multi-sweep technique becomes necessary. The first sweep is used to establish a pressure field for the entire domain. The term $\partial \bar{P}/\partial \xi$ is then used in the subsequent sweeps to relax and update the pressure field until a convergence criterion is met. Usually, the criterion is selected by the requirement that the maximum change in pressure from one sweep to the next be less than a specified tolerance for all the mesh points. The method is also known as the global pressure relaxation technique. When flow reversal in the streamwise direction is encountered, a simple procedure is to use the FLARE approximation of Reyhner and Flügge-Lotz [60]. A negative streamwise velocity (i.e., separated flow) will render the marching procedure to become unstable since the governing equations are again ill posed. The eigenvalue analysis in Ref. 57 indicates that when a flow reversal occurs the positive viscosity tends to amplify a disturbance instead of damping it. In the FLARE approximation one simply replaces the negative convection velocity with zero or a small positive number. The procedure works well only for flows with small separation bubbles; even if this is so, an additional procedure is required to make the

multi-sweep method stable [9]. Some results of the multi-sweep technique for nonreacting internal flows are shown in Ref. 9. For the present reacting-flow investigation, only the single sweep method will be used.

It should be noted that Eq. (3.18) is appropriate for a two-dimensional problem. For a three-dimensional problem, an approximate factorization technique may be needed in order to avoid inverting a sparse block matrix system of algebraic equations.

3.3 Boundary and Initial Conditions

Boundary and initial conditions are required for both elliptic and parabolized equations; they are discussed in the following subsections.

3.3.1 Conditions for Elliptic Equations

Before starting the time integration, initial distribution of dependent variables for all interior mesh points are specified using free stream values. This choice is very convenient since it requires no computation whatsoever and seems to work well for all problems investigated in this study. All characteristic values of the supersonic governing equations are positive indicating that the inflow conditions should be fixed whereas free outflow conditions could be used. In light of this, the inflow conditions are fixed at constant free stream values at all time steps. A method of extrapolation is employed at the outflow boundary. In this method, dependent variables at the exit boundary are equated to the variables at one station upstream of the exit, for a zeroth order extrapolation; first and second order extrapolations can be devised also. The method appears to work well even though it violates the rule of the method of characteristics within the subsonic layer close to a solid wall; this is probably because of the

thinness of the subsonic layer. At a solid wall, the no-slip conditions ($u = v = 0$) along with the adiabatic wall condition ($\partial T/\partial y = 0$) or specified wall temperature condition are imposed. Based on the analysis of boundary layer equations, the zero normal pressure gradient ($\partial p/\partial y = 0$) is also used at the solid wall; close examinations of numerical output reveals that this is indeed a good approximation. The non-catalytic conditions are used at the solid wall for all four of the species continuity equations. In this method, normal gradients of species mass fractions are set equal to zero since the condition requires no net diffusion of species into the wall. In the case where gaseous hydrogen fuel is injected from solid surfaces, the conditions of injected hydrogen are specified at mesh points within which lie the injectors. At a plane of symmetry, reflection boundary conditions are imposed.

3.3.2 Conditions for Parabolized Equations

Unlike the elliptic procedure, initial conditions (at the inflow boundary) have to be as accurate as possible. Any inaccuracy in initial conditions will jeopardize the accuracy of the solution through out the domain since the equations are steady and the method of solution is direct, without any relaxation. Any method can be used to specify the initial conditions insofar as it provides accurate variable profiles. In this study, the initial profiles are obtained from the results of the elliptic code. This may seem too restrictive since an elliptic problem has to be solved first before a parabolized investigation can be made. In real applications, the elliptic equations will be used only in the near field of the fuel injectors; the exit conditions of the elliptic results are then used as starting profiles for the parabolized code.

At a solid wall, the conditions imposed are the same as those used in the elliptic equations discussed in the previous subsection except that they have to be expressed in implicit delta forms compatible with the numerical algorithm. This is another advantage in using T as the intrinsic variable for the energy equation; if this is not so, the linearization of variable may be necessary in obtaining the implicit boundary conditions. Outflow conditions, however, are not needed since the solution is obtained by forward marching in the flow direction.

3.4 Numerical Dissipation Functions

It is well known that the central finite difference schemes, as used in this study, exhibits spurious numerical oscillations across a shock front. Without any control, the oscillation can destabilize the numerical scheme. To suppress this high frequency oscillation phenomenon, fourth-order dissipation functions are added to the righthand side of the elliptic algorithm (Eqs. 3.8-3.9) as follows:

$$f_\xi^4 = (\Delta\xi)^4 \frac{\partial}{\partial\xi} \frac{\xi_x^2}{J} (u + a) [C_1 \delta_\xi^2 P + C_2\delta_\xi^2 T] \frac{\partial}{\partial\xi} q \qquad (3.28)$$

$$f_\eta^4 = (\Delta\eta)^4 \frac{\partial}{\partial\eta} \frac{\eta_y^2}{J} (v + a) [C_1\delta_\eta^2 P + C_2\delta_\eta^2 T] \frac{\partial}{\partial\eta} q \qquad (3.29)$$

where

$$\delta_\xi^2 P = \frac{|P_{i+1,j} - 2P_{i,j} + P_{i-1,j}|}{P_{i+1,j} + 2P_{i,j} + P_{i-1,j}} \qquad (3.30)$$

$$\delta_\xi^2 T = \frac{|T_{i,j+1} - 2T_{i,j} + P_{i,j-1}|}{T_{i,j+1} + 2T_{i,j} + T_{i,j-1}} . \qquad (3.31)$$

42

The form of the functions were suggested by MacCormack [69]. In its original form, only the term $\delta^2 P$ was used; Drummond [70] found that for some problems this is not sufficient and suggested inclusion of the term $\delta^2 T$ as well. The coefficients C_1 and C_2 must be selected by numerical experiment. For the cases investigated in this study, both coefficients are fixed at a constant value of one-half; this value appears to work equally well for other problems. Finite difference representations of these smoothing terms follow the predictor-corrector sequence of the numerical algorithm.

For the value of the parameter C_c equals to zero, the parabolized code cannot be marched even for a single station since the diagonal term of the continuity equation is identically zero. To render the term non-zero as well as to provide some damping effects, the following third order implicit function

$$-C_I \ (\Delta\eta)^2 \ (\nabla_\eta \Delta_\eta) \Delta^n q$$

is added to the lefthand side of Eq. (3.18). A fourth order explicit function given by

$$-C_E A \ (\Delta\eta)^4 \ (\nabla_\eta \Delta_\eta)^2 \ q^n$$

is also added to the righthand side of the algorithm. The explicit term plays a major role in damping the oscillation. A simplified Von Neumann analysis shows that both C_I and C_E must be positive (but note the minus signs in front of the coefficients). The value of C_E must not be larger

than 1/8 for stability reasons. For large value of C_I, however, the stability bound of C_E increases to about one-half of C_I. An algebraic relation for which optimal damping of high frequency oscillation is attained is given by

$$1 + 4 \, C_I - 16C_E = 0 \qquad (3.32)$$

It is suggested that C_I be selected first and C_E determined such that the above relation is satisfied. By numerical experiments it is found that $C_I = 1/4$ and $C_E = 1/8$ gives the best results at least for the cases considered in this study. Different smoothing funtions for this type of algorithm can be found in [9, 71, 72]. It should be noted that the explicit function has the Jacobian matrix, A, in multiplication whereas the implicit function does not. The Jacobian matrix is included to mimic the form of the linearized streamwise flux. Inclusion of the Jacobian matrix in the implicit function would destroy its diagonal-dominance effect for which the term is added. Numerical experiment indicated that Jacobian scaling of the explicit function does give a better smoothing effect than without the scaling.

3.5 Grid Generation

An algebraic grid generation technique similar to that developed by Roberts [73] is used to obtain computational grids. By using the grid generation technique, a physical domain is transformed into a rectangular computational domain with uniform mesh spacing. The size of the computational mesh is arbitrary; in this study, it was selected to be unity. Working with the rectangular computational domain is much simpler than with the skewed physical domain since finite difference representations of derivatives and

implementation of boundary conditions become fairly straight forward without having to resort to interpolations.

The technique allows clustering of mesh points near boundaries in order to resolve high gradient quantities. Clustering can be made either at one end or both ends of the coordinate. An algebraic stretching function can be given as:

$$S = N1 + \frac{(N2 - N1)}{2} \frac{\left[(\beta+2\alpha)\ \sigma - \beta+2\alpha \right]}{(2\alpha+1)(1+\sigma)}$$ (3.33)

where N1 is the smallest coordinate index and N2 is the largest coordinate index. If the parameter α is equal to zero the mesh near N1 will be clustered; the mesh near both N1 and N2 are clustered if α is equal to one half. The degree of clustering is controlled by the magnitude of β. The closer the magnitude of β is to unity from above the more the clustering will be. The quantity σ is a variable defined by

$$\sigma = \left[\frac{(\beta + 1)}{(\beta - 1)} \right]^{\frac{\theta-\alpha}{1-\alpha}}$$ (3.34)

where θ is a variable ranging from zero to one and is given as

$$\theta = \frac{N-N1}{N2-N1}$$ (3.35)

where N ranges from N1 to N2.

The magnitude of the physical coordinate at each mesh point can now be

45

obtained by the relation (the normal coordinate, y, is given here for illustrative purpose):

$$Y_N = [Y_{N2} (S_N - N1) + Y_{N1}(N2 - S_N)]/(N2 - N1) \qquad (3.36)$$

where the subscript N denotes the index of the mesh point in question. The stretching of the physical coordinate in the streamwise direction, if desired, can be achieved in a similar fashion. No attempt has been made to enforce orthogonality of the grid system. Orthogonality is not very critical since the geometries of interest do not vary appreciably in the normal direction.

The mesh spacing near a solid wall is governed by the Reynolds number of the flow. In order to properly resolve the details within a laminar boundary layer, the minimum mesh spacing close to the solid wall should approximately satisfy the following relation [69]

$$\Delta Y_{min} = \frac{2}{3} \frac{L}{Re_L^{0.5}} . \qquad (3.37a)$$

For a turbulent boundary layer the relation is given by

$$\Delta Y_{min} = \frac{100 \ L}{Re_L^{0.9}} . \qquad (3.37b)$$

This is achieved by varying the parameter β and can, at best, be a trial and error process.

Figure 3.1 shows a 31x31 grid system for a problem solved in this
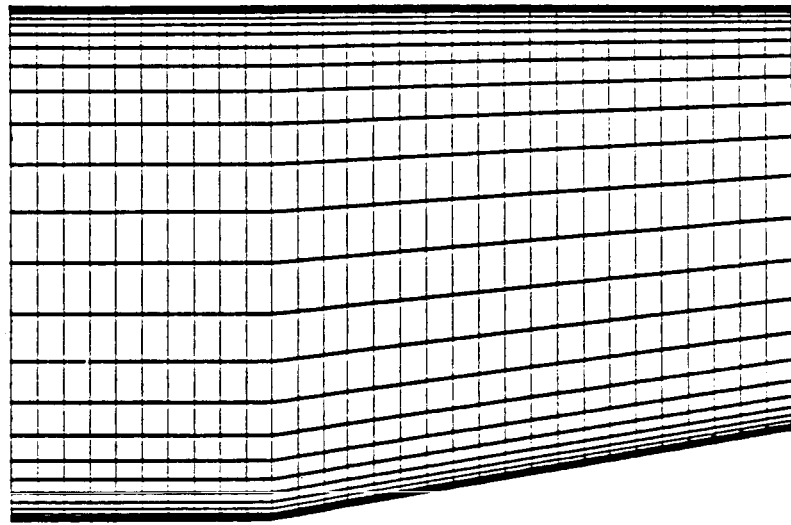
Fig. 3.1 Grid structure of case No. 1.

study. It can be seen that only the normal coordinate is clustered. Clustering of mesh point in both normal and streamwise directions is illustrated in Fig. 3.2. This is a 87x60 grid used in the other problem that is investigated.

3.6 Solution Procedures

Some important procedures used in the computer codes for obtaining the solution are discussed in this section.

3.6.1 Procedures for Elliptic Code

The elliptic computer code is written specifically for the VPS-32 vector processing computer at the NASA Langley Research Center. The fluid dynamic equations are integrated in time from an initial solution by the fully explicit unsplit MacCormack finite difference algorithm. The species equations give rise to a block mono-diagonal system of algebraic equations which can be solved very efficiently on the VPS-32 computer. The LU decomposition is applied on these blocks one element at a time. Elements of matrices which have the same species indices are traced through spatial indices vectorially throughout the domain. Without this technique, the code was quite expensive to use (about one hour of CPU time on the VPS-32 computer). With the present technique implemented, however, the total CPU time was reduced to about 800 seconds on the same test case whereas mixing along (without combustion) required some 600 seconds. The vectorized subroutines that solve the block diagonal system are given in Appendix C.

Once all the conservative variables are obtained at a time step, the primitive variables have to be extracted. Some difficulties arise in deciphering the temperature, T, since it is embedded in $\rho H-p$, the intrinsic dependent variable of the energy equation. This study assumes that the
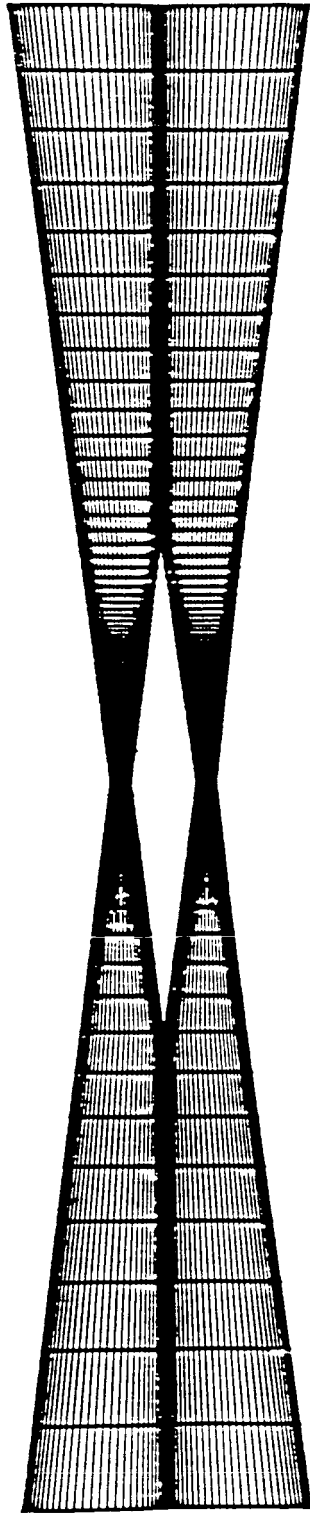
Fig. 3.2 Grid structure of case No. 2.

specific heat, $\bar{C}_p$, and the gas constant, $\bar{R}$, of the mixture can be lagged one time step without causing any significant error. With the above assumption, temperature can be obtained as follows

$$T = [(\rho H - p) - \frac{1}{2} \rho (u^2 + v^2) - \sum_{i=1}^{5} f_i H_i^\circ]/(\rho \bar{C}_p^* - \rho \bar{R}^*) \qquad (3.38)$$

where the starred quantities are to be evaluated at the old time level. By using Eq. (3.38) the temperature of the new time level can be obtained directly without having to solve a second order algebraic equation in T. The time step used is determined from the CFL condition:

$$\Delta t = (\sigma) \min [\frac{\Delta x}{|u|+a}, \frac{\Delta y}{|v|+a}] \qquad (3.39)$$

where σ is the CFL number of magnitude less than one. Note again that use of this large time step is possible only if the chemistry source terms are evaluated implicitly. If an accurate temporal history is desired, one must choose Δt in a different manner (see, e.g., Ref. 21). Experiences gained during the numerical experimentation have suggested that the value of σ should be small in the early phase of time integration. The magnitude of σ is then gradually brought up to 0.9 in about 100 time steps. Attempts to use $\sigma = 0.9$ at the very beginning yielded negative temperature which was probably due to a relaxation process that was too abrupt.

Unlike the conventional central difference scheme, the present numerical scheme lacks a decisive, so called, residual to be monitored for a convergence criterion. A steady state solution is determined by monitoring

50

the following criteria:

1. The maximum change in density for all mesh points from a time step to the next be less than a specified tolerance.

2. The L -norm of the change in density from a time step to the next be less than a specified tolerance.

3. The total integration time is equal to or greater than the time required for a fluid particle with free stream velocity to travel three times the length of the physical domain.

The tolerances for the first two criteria are usually selected as numbers of three to four orders of magnitude smaller than the changes of corresponding quantities over the first integration step. Most importantly, the numerical solution must be examined in detail by appropriate measures for physical plausability.

3.6.2 Procedures for Parabolized Code

The parabolized code was developed in a standard FORTRAN4 language. Initial solution profiles are needed to start the program. The profiles were obtained from solution of the elliptic code as discussed earlier. For the present two-dimensional problems, the storage requirement of the program is equivalent to that of a one-dimensional problem. Ironically, the coding chore is more laborious than the elliptic code couterpart due to its fully-implicit fully-coupled procedure. Two levels of data are needed to obtain a solution at the next station. Only one level of data is used to start up the program; this is done by using a first order scheme by specifying a=1 and b=0. Attempt has been made to start up with two levels of data by a second order scheme; however, this results in instability due probably to the fact that the two level initial data contained too much elliptic infor-

mation.

Unlike the elliptic code, the temperature, T, is computed directly; this eradicates the need to decipher T from a related variable. Some difficulties arise in evaluating the Jacobian matrix of the chemistry source terms since the kinetic rate constants are strong and complicated functions of temperature. The difficulties are alleviated by lagging the temperature of the kinetic rate terms; this does not seem to affect the quality of the solution.

The block (8x8) tri-diagonal system of algebraic equations are solved by a direct non-iterative procedure. The so-called Thomas algorithm in conjunction with an LU decomposition procedure is employed in inverting these block matrices. There is no convergence criteria for the code since it is a single sweep method. If the situation warranted, a multi-sweep procedure could be implemented very easily. It is recommended that the number of sweeps be limited to only a couple of times; too many sweeps will certainly make the code less attractive. Fortunately, the physical problems for which the present parabolized formulation is applicable (supersonic high Reynolds number flows) almost always guarantee that only a couple of sweeps are indeed necessary [9].

4. RESULTS AND DISCUSSION

Results of the elliptic code are presented first followed by the results of the parabolized code.

4.1 Results of Elliptic Code

To gain some confidence with the elliptic code, a simple geometry problem was solved first. The flow conditions and the geometry of the test case are depicted in Fig. 4.1. A 31x31 grid system as shown in Fig. 3.1 was
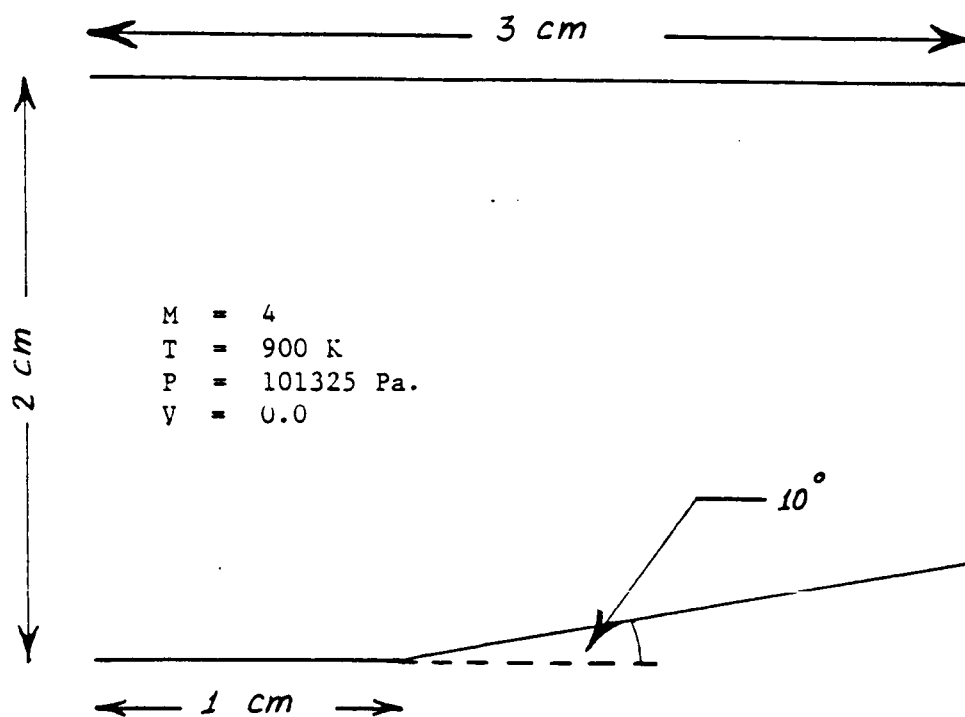
Fig. 4.1 Geometry and flow conditions of case No. 1.

used in this test case. This is a premixed case with an equivalence ratio (ϕ) of unity. The inflow temperature of the mixture was arbitrarily selected as 900 K in order to study the effect of the explicit ignition switch incorporated in the program. As mentioned earlier, the reaction is not allowed to take place when the temperature is lower than 1000 K; it is to be expected, then, that reactions should occur only behind the shock wave and within the adiabatic boundary layers where temperature goes beyond 1000 K. Figures 4.2 and 4.3 show the concentration contours of OH species and H_2O species, respectively. The contours indicate reacted regions as expected. The line plot in Fig. 4.4 illustrates distributions of various species along the y-location of about 0.13 cm from the lower wall (y-station No. 15). It is seen that the OH concentration increases rapidly across the shock wave and stays relatively constant thereafter (at its equilibrium value). The H_2O concentration, however, increases continuously signifying that more fuel is being consumed by an exothermic process. The behavior of the species distributions is in good accordance with the physics of the global two-step chemistry model used. A similar plot at the lower-wall surface is given in Fig. 4.5.

The geometry of a more realistic problem and its inflow conditions are shown in Fig. 4.6. The geometry and flow conditions are representative of a planar cut perpendicular to the inward swept leading edge of a three-dimensional single strut scramjet engine. It is noteworthy that this is the same configuration used in the study of Drummond and Weidner [74]. Gaseous hydrogen fuel is injected into the flow from the side walls and from the center strut such that the overall equivalence ratio is equal to one. The conditions of injected hydrogen are: $p = 258706$ N/m^2, $T = 246$ K, $u = 156$ m/sec, $v = 1241$ m/sec. The injectors are located 6 cm downstream of the

CONTOUR FROM   0.   TO   .10800
     CONTOUR INTERVAL IS   .60000E-02
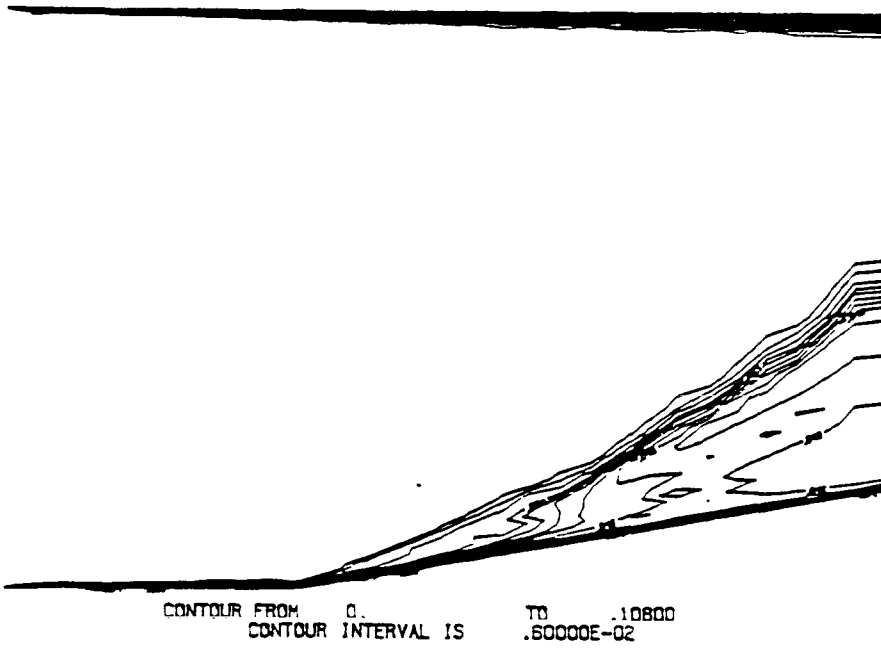
Fig. 4.2   OH concentration contours.

CONTOUR FROM   C.   TO   .14400
CONTOUR INTERVAL IS   .90000E-02
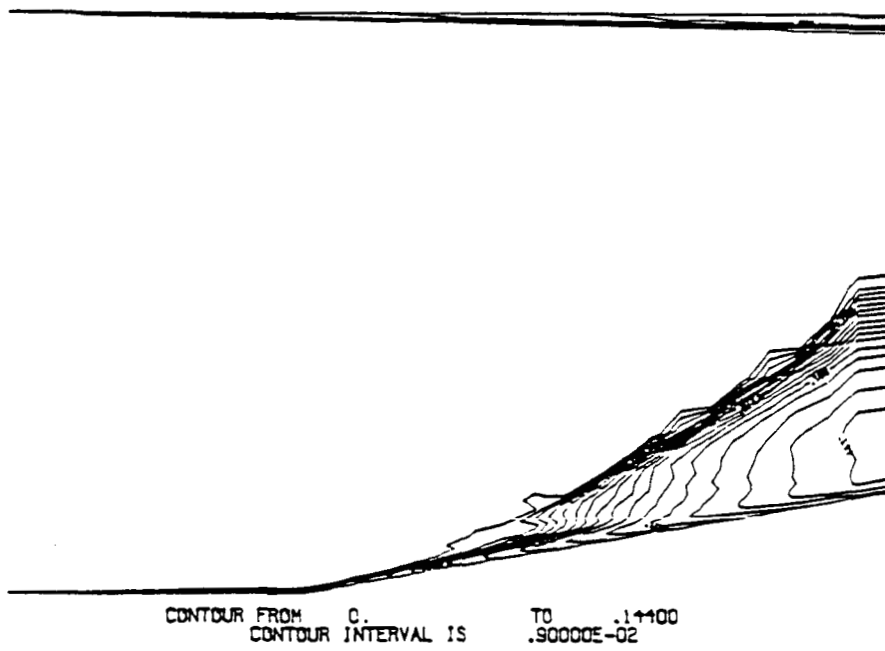
Fig. 4.3 H_2O concentration contours.
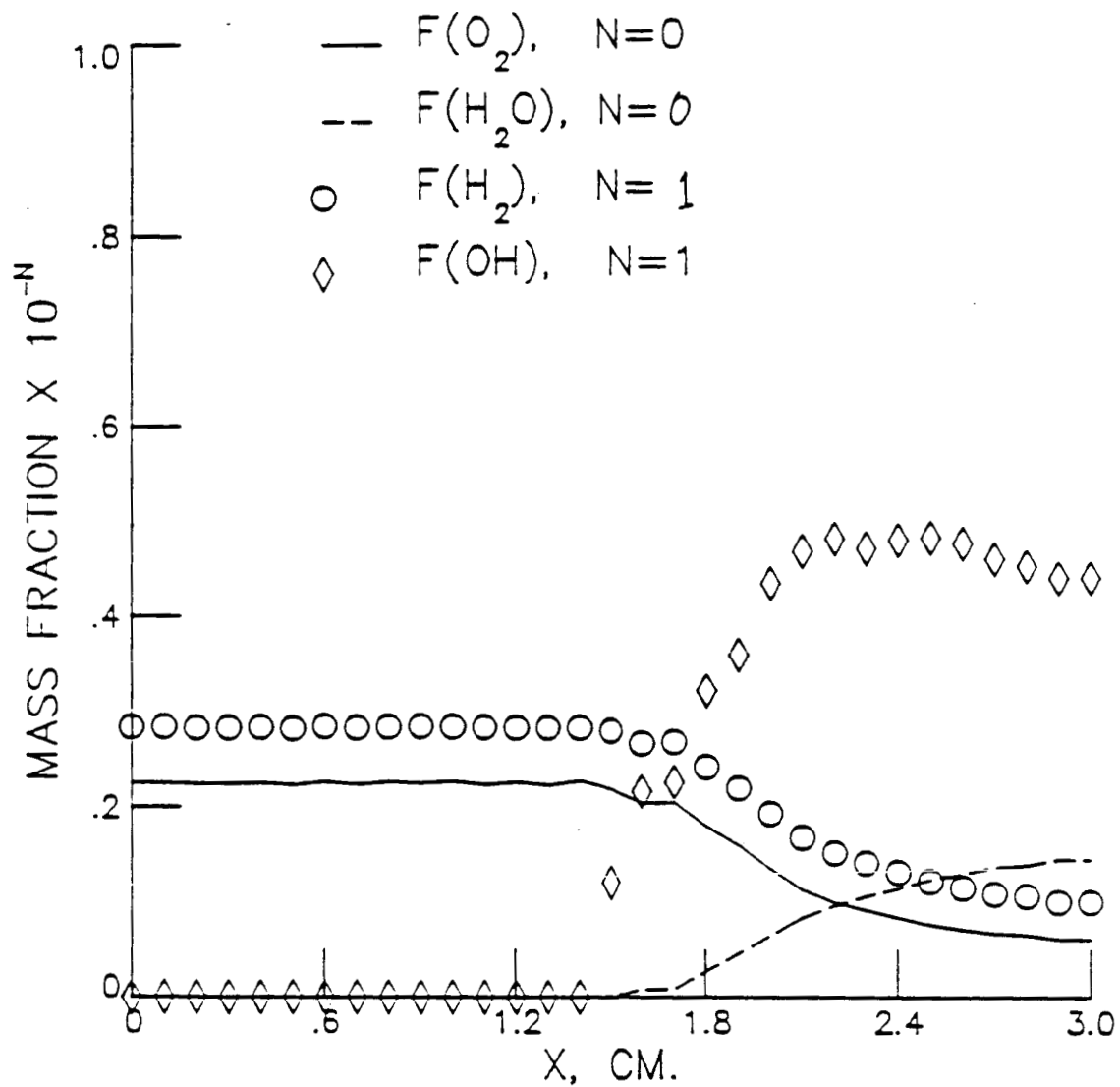
Fig. 4.4 Distribution of species mass fraction along y-station No. 15.
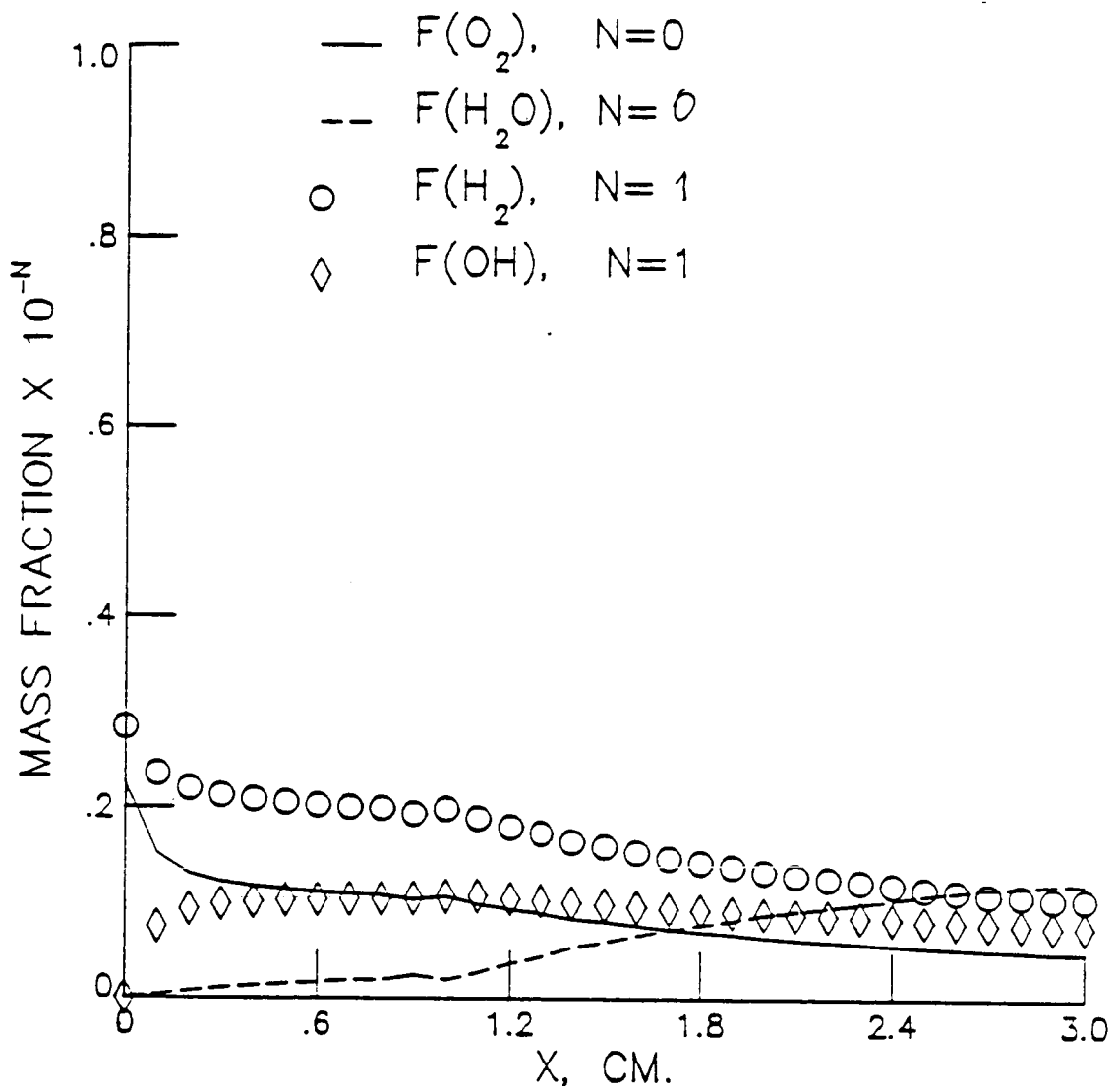
Fig. 4.5 Distributions of species mass fraction at the lower wall.

Inflow conditions :

T = 335 K
N = 5.07
P = 3546 Pa.
V = 0.0

injectors

strut

← 15 cm →

25.8 cm

78 cm
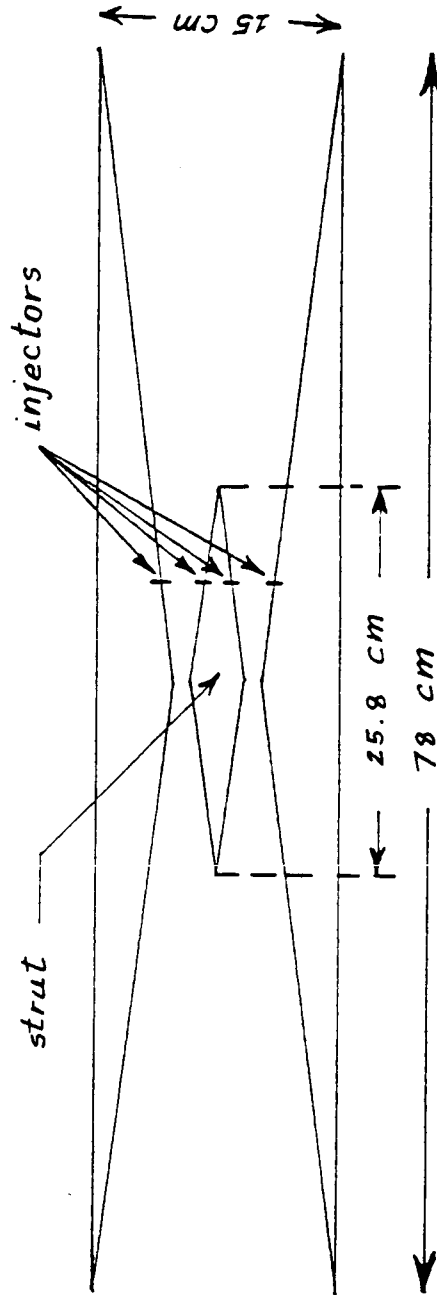
Fig. 4.6 Geometry and flow conditions of case No. 2.

engine cross sectional minimum and are each 0.1 cm wide. Due to symmetry, only the upper half of the domain is solved. A grid system of 87x30 is employed. Grid points are concentrated near the solid surfaces in the y-direction and near the injectors in the x-direction (see Fig. 3.2). Clustering of mesh points in the near field of the injectors is necessary to properly resolve jet-flow interaction and the mixing process between the fuel and air. The computational grid used is the same as that of Ref. 74 in order to allow point by point comparisons of the results.

It is of interest to study the nonreacting (mixing only) case first so that the inferences can be made later on as to the effects of combustion on the flow field. Figures 4.7-4.9 show the pressure contours, velocity vectors, and H_2 concentration contours, respectively, for the nonreacting case. The figures reveal that small separation bubbles occur before the throat due to interactions of shock waves and boundary layers. Separations also occur immediately upstream of the injectors; it is imperative to have these separations for proper flame holding in the engine.

Results with chemical reactions are given in Figs. 4.10-4.15. Figures 4.10-4.12 illustrate the similar information to that in Fig. 4.7-4.9. It is seen from Fig. 4.11 that the separation bubbles upstream of the throat increases in size as compared to the nonreacting case. This is believed to be due to a higher level of back pressure caused by the heat release from combustion. The separation bubbles, in turn, induce upstream shock waves as can be seen in Fig. 4.10. The occurrence of these bubbles due to inlet-combustor interaction can easily choke the flow in the inlet and should be avoided, if possible, in design. The hydrogen contours shown in Fig. 4.12 indicate that the fuel jets do not penetrate significantly into the core air flow resulting in low level of mixing. Increasing the jet pressure and
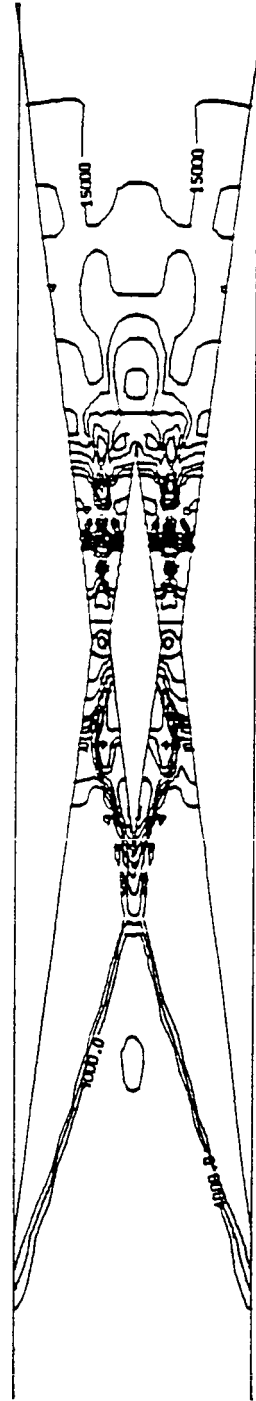
Fig. 4.7 Pressure contours of nonreacting case.
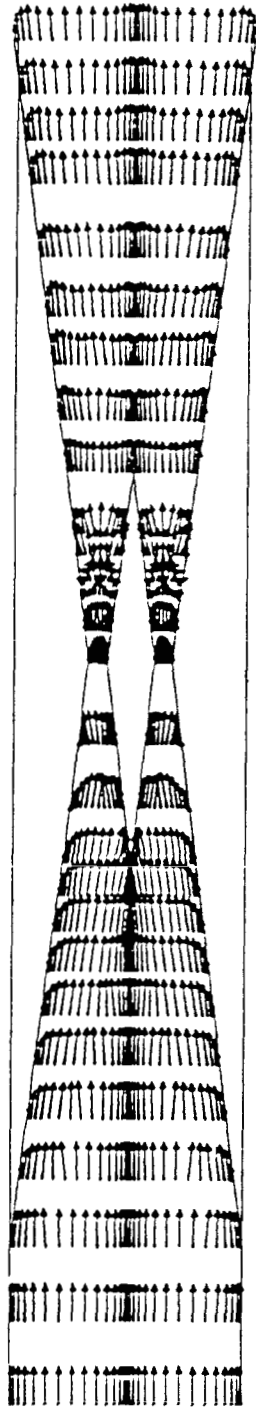
Fig. 4.8 Velocity vectors of nonreacting case.
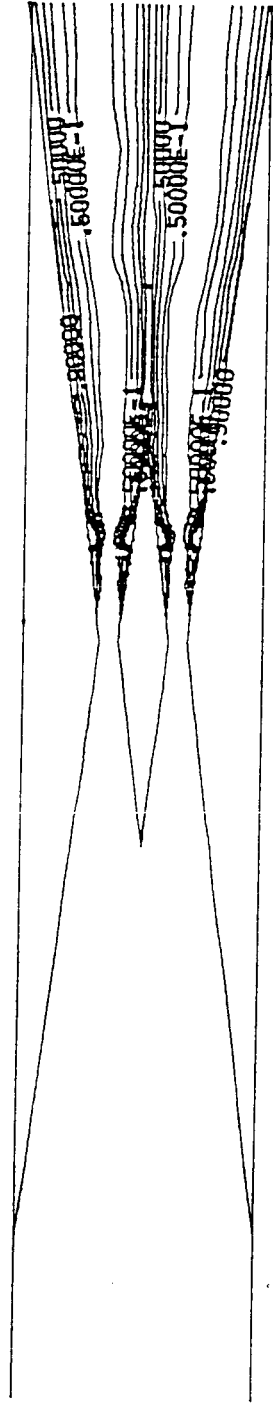
Fig. 4.9 H_2 contours of nonreacting case.
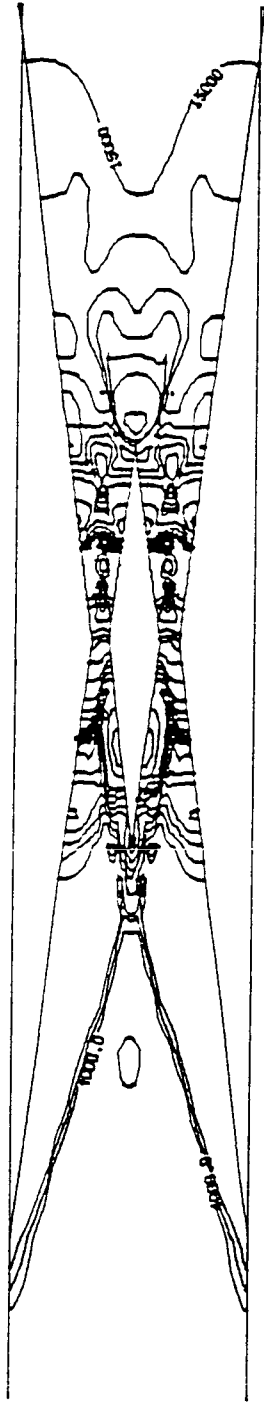
Fig. 4.10   Pressure contours of reacting case.
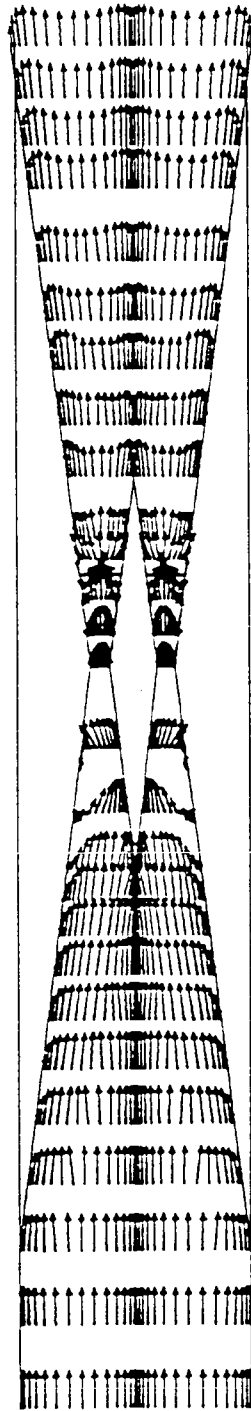
Fig. 4.11 Velocity vectors of reacting case.
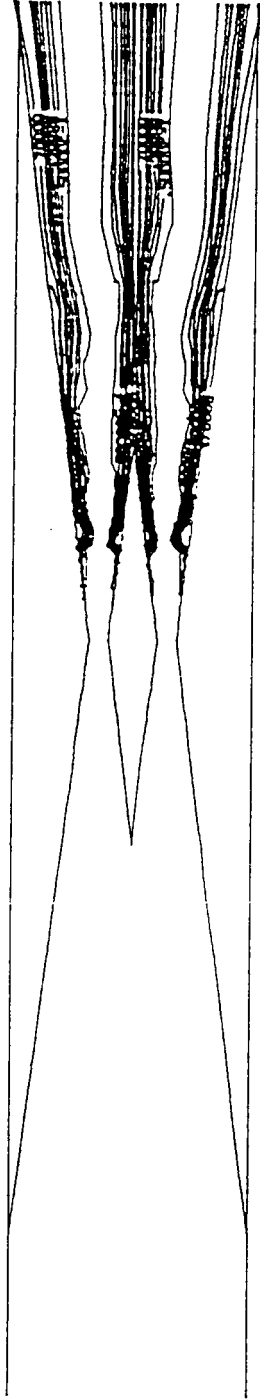
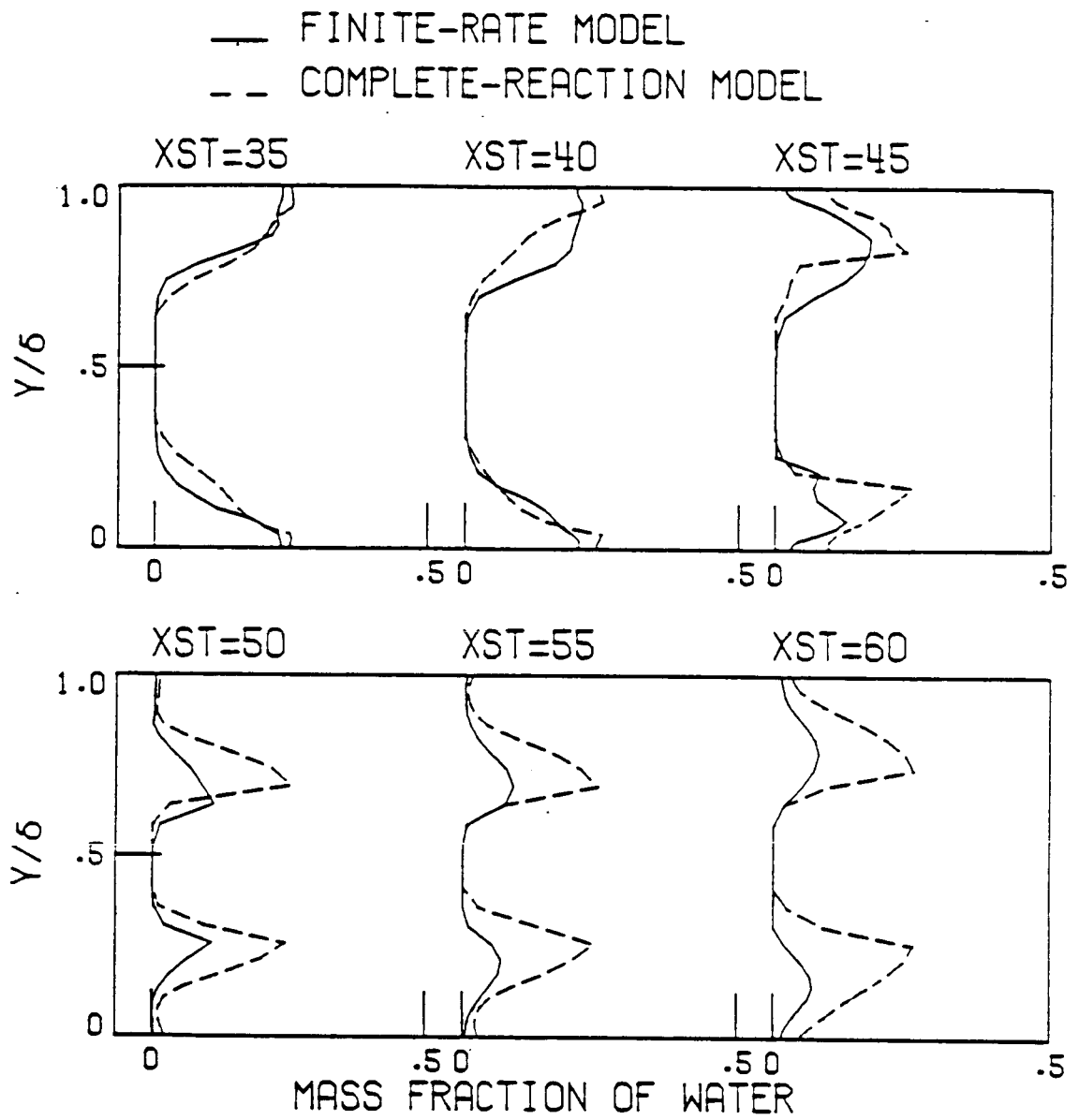Fig. 4.12 H_2 contours of reacting case.
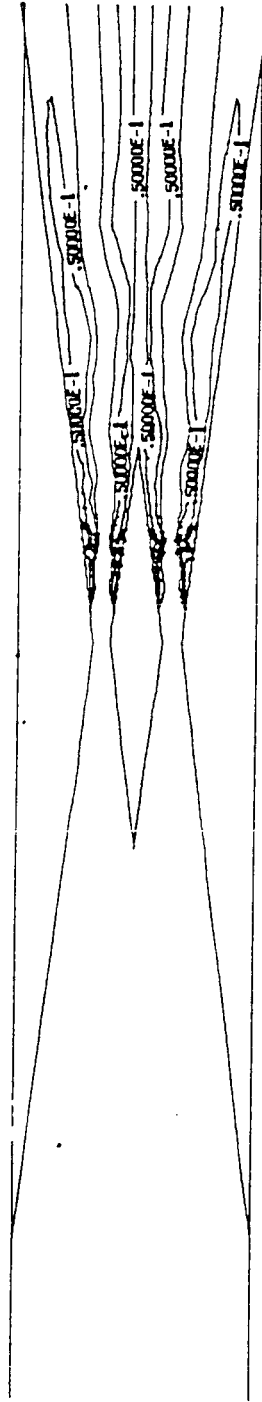
Fig. 4.13 H_2O contours of reacting case.
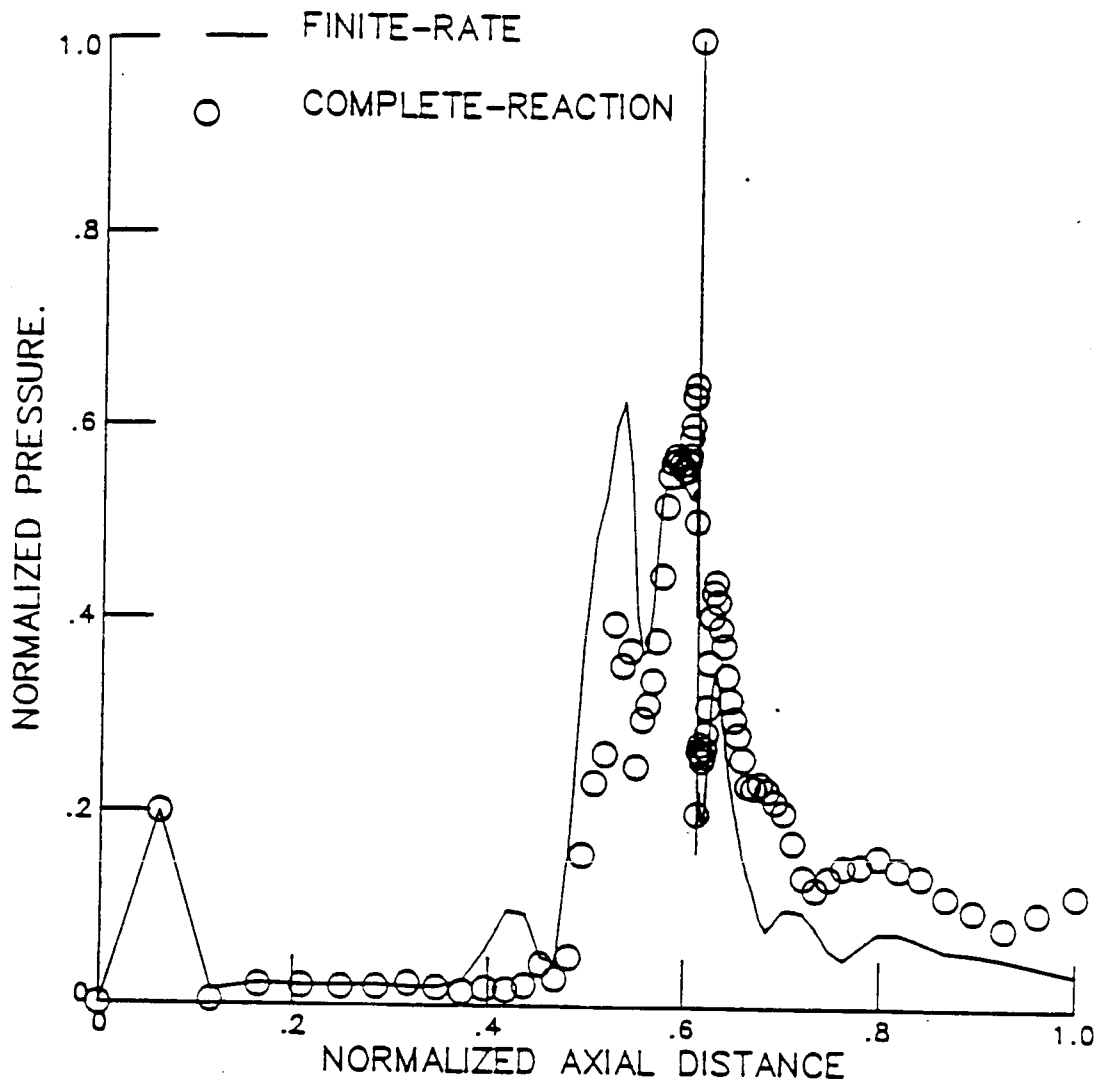
Fig. 4.14 Cross stream profiles of H_2O mass fraction.

Fig. 4.15 Upper surface pressure distributions.

velocity can, again, choke the flow. Parametric studies of the jet conditions required to promote more mixing will be the subject of future study. Figure 4.13 shows the water concentration contours of the reacting case indicating the regions where combustion has taken place.

One major purpose of this study has been to compare the extent of combustion using the present finite rate chemistry model with the results of Drummond and Wiedner [74] where a complete reaction model was used. In the complete reaction model, only the species equation for the fuel is solved along with the fluid dynamic equations. There is no source term in the fuel species equation and therefore the system is not stiff. The extent of combustion is determined by assuming that when the fuel and oxidizer mix at temperatures above 1000 K they react to their maximum extent possible (stoichiometric limit) until one reacting partner is completely depleted.

The comparisons of water profiles at some selected x-stations are made in Fig. 4.14. The cross stream coordinate at each station was normalized with the corresponding channel's width such that its value ranges from zero to one. The top graph shows the profiles upstream of the injectors within the recirculating zones where flames are stabilized. It is seen that the concentration levels of water, which are an indication of the extent of combustion, are approximately the same. This could be attributed to the fact that mixture velocity in the recirculating zones is relatively small providing ample resident time for it to react to an appreciable amount. The bottom graph of Fig. 4.14 indicates the water profiles downstream of the injectors where it can be seen that the finite rate model predicts a lower level of combustion than the complete reaction model. This is consistent with the formulation of the two models since the finite rate scheme does not necessarily allow complete reaction.

70

Finally, normalized surface pressure, $(p-p_{max})/(p_{max}-p_{min})$, is plotted in Fig. 4.15. The highest spike in the plot indicates the location of the injector. The finite rate model predicts a small bump in surface pressure upstream of the cross sectional minimum whereas the complete reaction model does not. This pressure bump was caused by the induced shock wave ahead of the separation bubble; the complete reaction model does not show as large a separation. Downstream of the injector, however, the pressures exhibit similar trends except that the pressure predicted by the complete model is somewhat higher due mainly to a greater degree of combustion.

4.2 Results of Parabolized Code

All results reported in this section were obtained by using the single sweep method with the value of ω equals to 0.7. In most cases, the values of important parameters used are indicated at the bottom of the figures.

The premixed test case (Fig. 4.1) solved earlier by the elliptic code has been reinvestigated by the parabolized code. Initial data profiles were obtained from those of x-station No. 5 of the elliptic results which is located at five stations upstream of the compression corner. Regardless of the schemes used, the code is always started up by the Euler implicit scheme which requires only one level of initial data. In the following discussion, comparisons are made between results of the parabolized and elliptic codes.

Results obtained by using the second order accurate three point backward scheme are illustrated in Figs. 4.16-4.18. Comparisons of temperature and pressure between the parabolized (PNS) and elliptic (NS) results are made in Fig. 4.16. The plots are made along the y-station located approximately 0.13 cm from the lower wall (y-station No. 15). It can be seen that the comparisons are very reasonable. In the absence of combustion, the
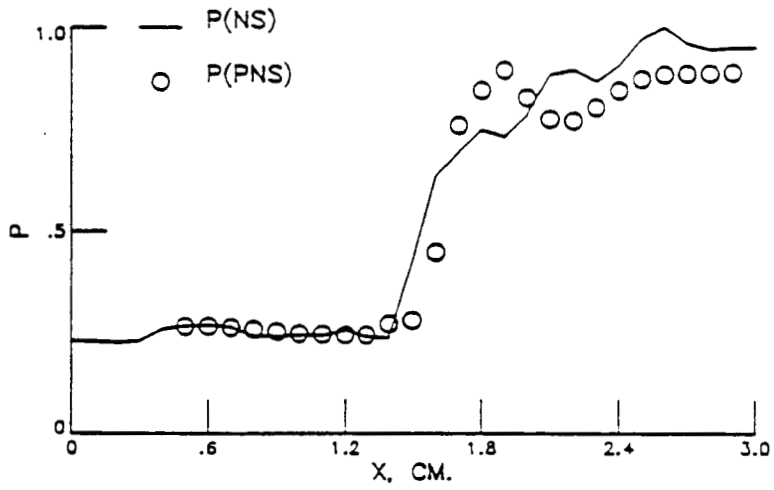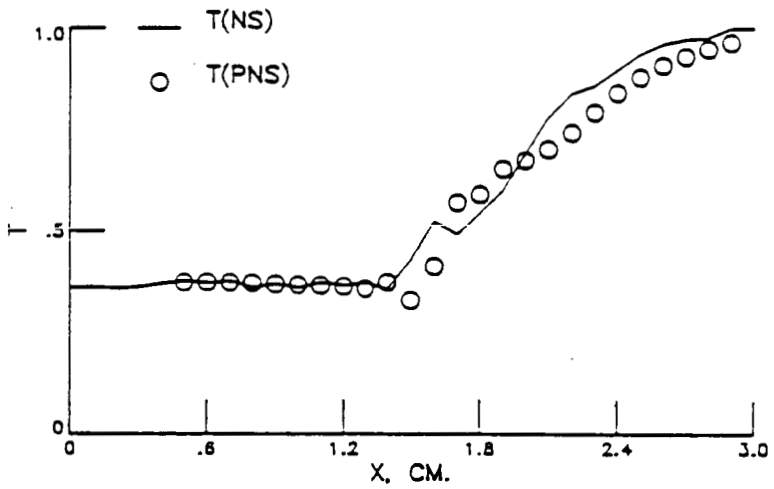
Fig. 4.16 Temperature and pressure along y-station No. 15, three-point-backward scheme.
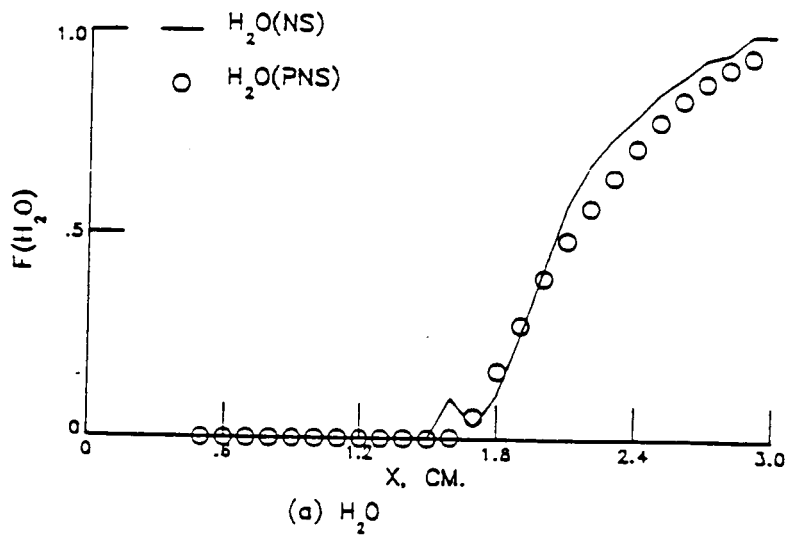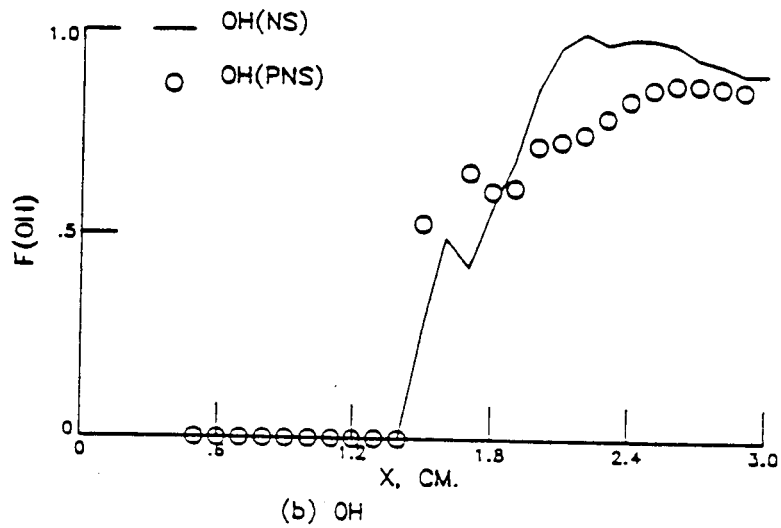
Fig. 4.17 H_2O and OH mass fraction along y-station No. 15, three-point-backward scheme.
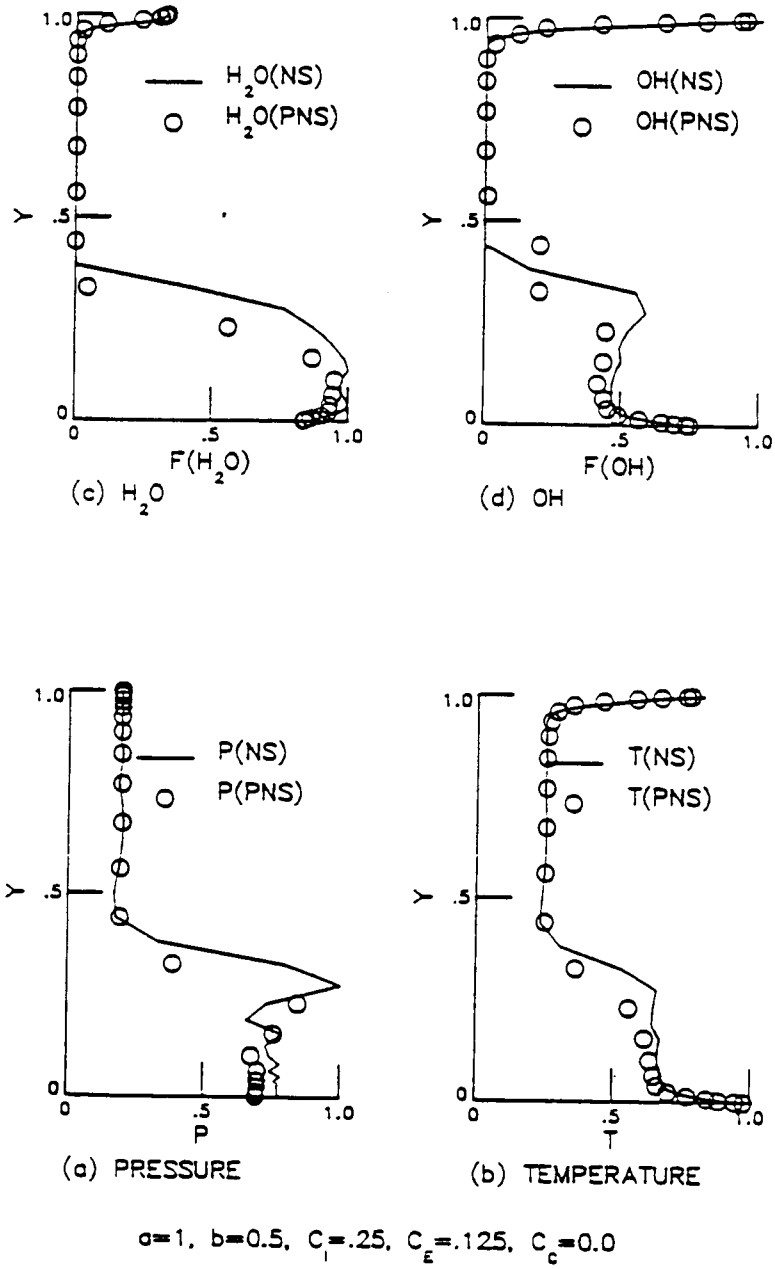
Fig. 4.18 Cross stream profiles at the outflow boundary for various variables, three-point-backward scheme.

pressure and temperature behind the shock wave would remain constant. Increase in pressure and temperature due to heat release during combustion are predicted very well by the PNS code. Both NS and PNS results show some oscillations in pressure. Use of parameter C_c = 0.2 and/or larger values of the smoothing coefficients do not suppress these oscillations. The distributions of H_2O and OH species along the same y-station are compared next in Fig. 4.17. The H_2O mass fractions compare well for both formulations but the OH mass fractions show some disagreement. In fact, OH mass fraction in the PNS results at the grid point right at the shock front takes a huge jump out of the plot frame. Fortunately, the jump occurs at only one grid point and appears to be a very local phenomenon. By refining the mesh spacing in the streamwise direction two times, however, the jump disappears as indicated in Fig. 4.19. It is, therefore, concluded that the jump in OH species (which is the one that causes chemical stiffness) occurs because of large linearization errors due to the use of a coarse mesh. Even with the refined mesh, the PNS results underpredict the OH mass fraction when compared with the NS results (Fig. 4.19). The discrepancy is believed to be due to the lagged temperature used in the evaluation of the Jacobian matrix for the chemistry source terms. As the flow develops further downstream, however, OH concentration picks up to the same level as the NS results. Figure 4.18 details the comparisons of various quantities across the channel at the outflow boundary of the geometry. The cross stream coordinate, Y, was normalized such that its value ranges from zero to one whereas the dependent variables are scaled with respect to their corresponding maximum values. All profiles appear to be in reasonable agreement. Both results suffer oscillation in pressure across the shock front which is typial of a central difference scheme. Not shown here are the velocity profiles; numerical
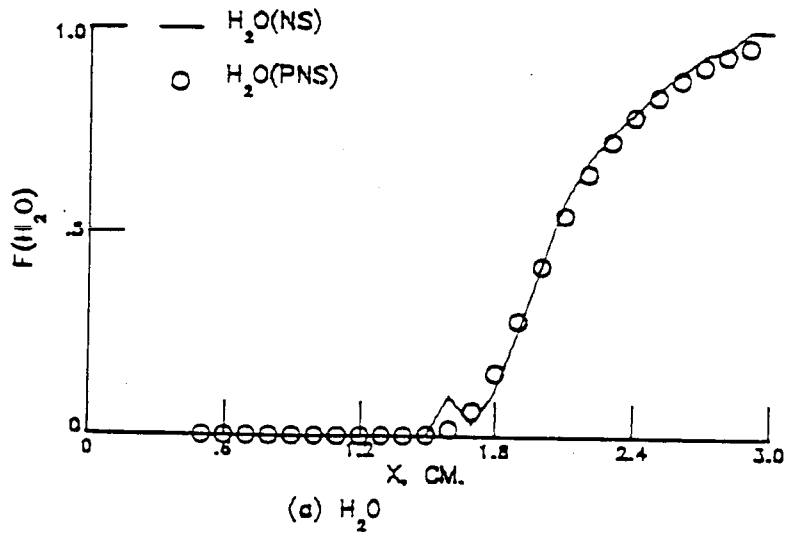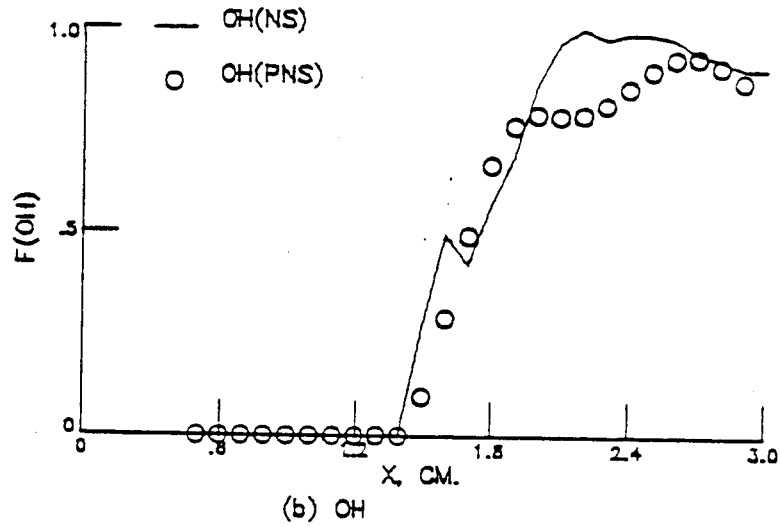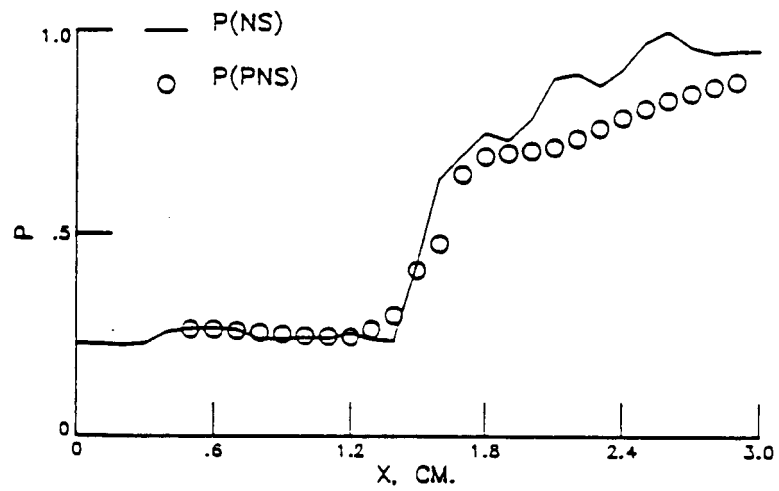
Fig. 4.19 H_2O and OH mass fractions along y-station No. 15 with refined mesh spacing.

output indicates that velocity profiles for the two formulations are in good agreement.

Figure 4.20-4.22 show the same information as those of Figs. 4.16-4.18 but the new figures were produced by using the first order accurate Euler implicit scheme. Note that the value of C_c is equal to 0.2 rather than zero. The vanishing of C_c for this scheme cannot be allowed since it gives rise to an instability regardless of the magnitude of the values of the smoothing coefficients; this appears to be the case only for reacting flows since zero value of C_c was used all the time in nonreacting flow calculations [8, 9]. A jump in OH concentration across the shock front persists as in the three point backward results. In general, these plots indicate that results of the Euler implicit scheme are slightly inferior to those of the three point backward scheme.

The single strut scramjet engine problem is also reinvestigated with the PNS code. The x-station No. 59 was selected as the starting solution; this is reasonably well downstream of the injectors where elliptic effects should be weak. Like the previous case, only the one-level Euler implicit scheme is used to start up the integration. In all the plots to be discussed, the symbol always indicates the PNS results whereas the solid line represents the NS results. Figures (a) always indicate surface pressure whereas Figs. (b), (c) and (d) always indicate cross stream pressure at the outflow boundary (x-station No. 85), cross stream pressure at x-station No. 70 and cross stream mass fractions of H_2O at x-station No. 70, respectively. All variables are scaled with respect to their corresponding maximum values and the spatial coordinates are normalized such that their values range from zero to one.

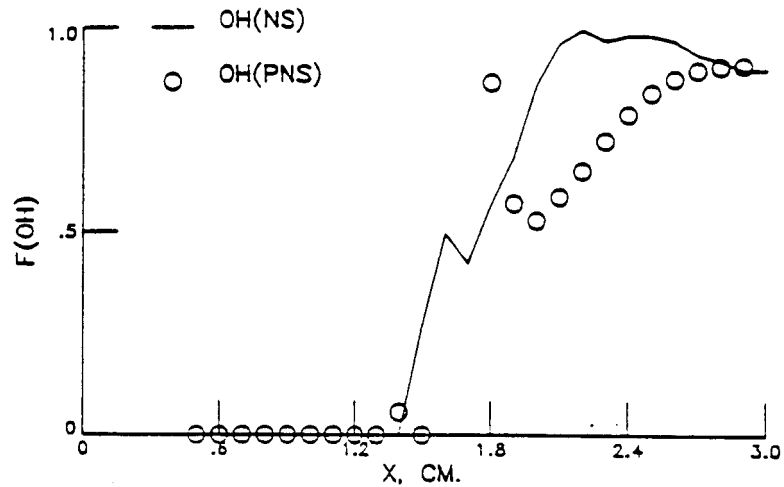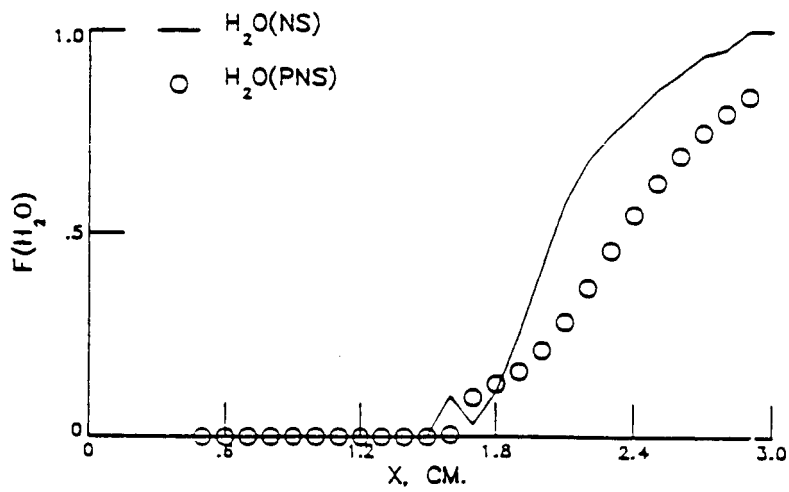Results of the three point backward scheme are shown in Fig. 4.23. It
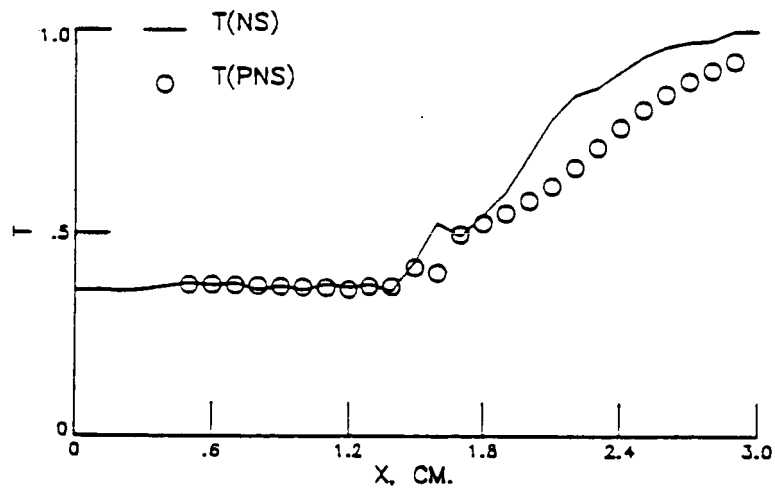
Fig. 4.20 Temperature and pressure along y-station No.15,
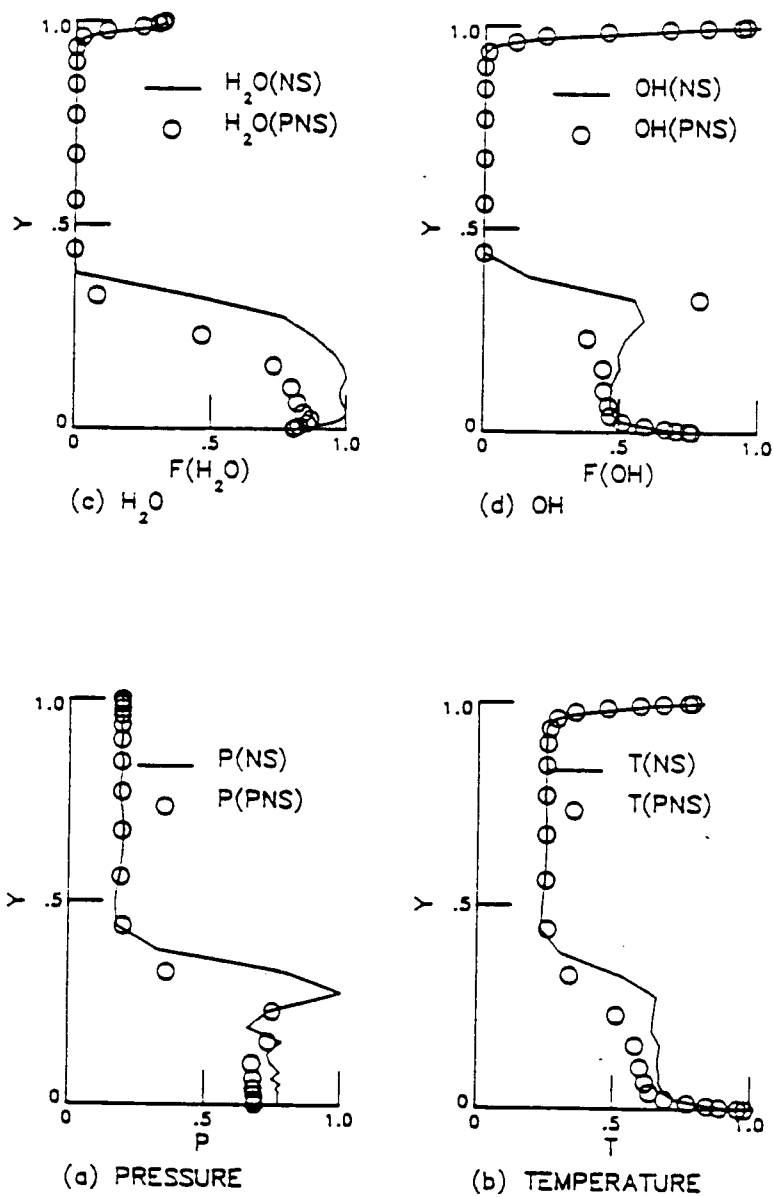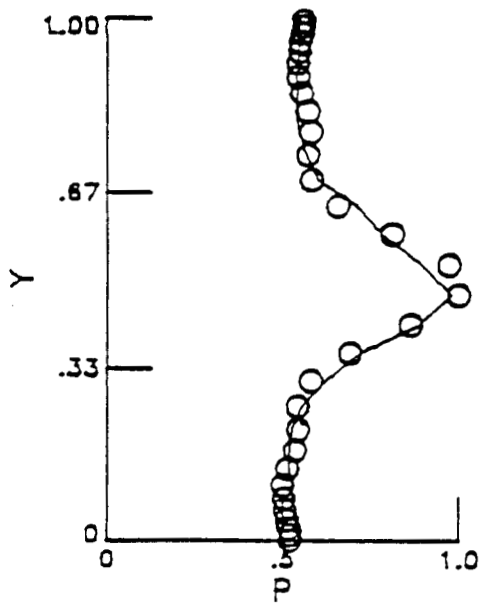Euler implicit scheme.

(b) OH

(a) H_2O

$a=1$, $b=0.0$, $C_i=.25$, $C_E=.125$, $C_c=0.2$

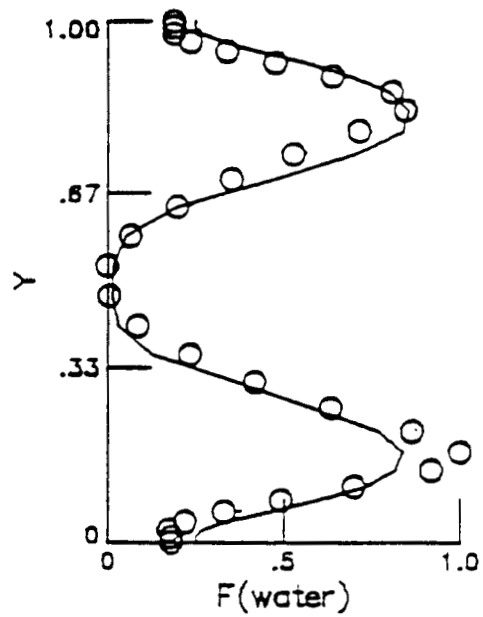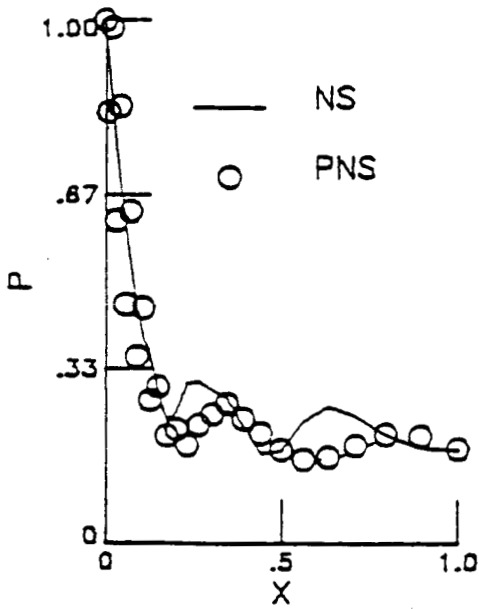Fig. 4.21 H_2O and OH mass fractions along y-station No. 15, Euler implicit scheme.

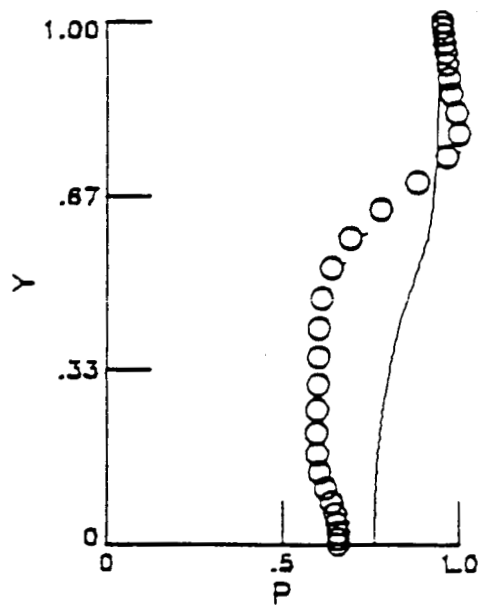Fig. 4.22 Cross stream profiles at the outflow boundary for various variables, Euler implicit scheme.

(c) P AT XST=70

(d) H$_2$O AT XST=70
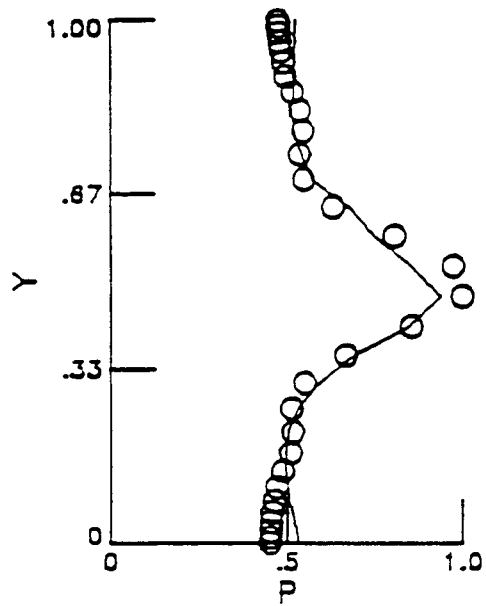
(a) SURFACE P

(b) P AT XST=85

a=1, b=0.5, C$_I$=0.25, C$_E$=0.125, C$_c$=0.0

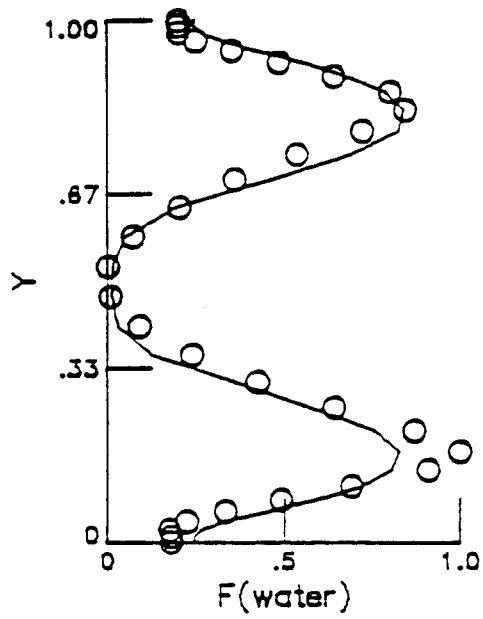Fig. 4.23 Results of three-point-backward scheme (No. 1).

is seen that the early phase of surface pressure (Fig. 4.23(a)) is oscillatory. The cross stream variables at x-station No. 70 compare very well with the NS profiles but the cross stream pressure at x-station No. 85 is not in good agreement. By using $C_c = 0.2$, the oscillation in surface pressure disappears as can be seen in Fig. 4.24(a). However, quality of other variables is slightly degraded; this is probably due to the fact that a non-zero C_c disrupts the second order accuracy of the scheme. Larger values of C_c worsen the PNS solution even further but the surface pressure becomes smoother. Increasing the values of C_I and C_E, while using $C_c = 0$, however, appears to improve solution of the PNS code as is evident from Figs. 4.25 and 4.26.

Results obtained by using the Euler implicit scheme are presented in Figs. 4.27-4.29. As in the previous problem, the scheme becomes unstable for the value of C_c equals to zero. In general, the results shown in these three figures are superior to the results of the three point backward scheme. This surprising paradox was reported earlier by Chitsomboon et al. [9] is solving nonreactiong flows. It appears that the Euler scheme has more natural damping capability embedded in it since the first truncated term in the scheme is an even order term (second-order derivative) whereas the three point backward scheme has an odd order term (third-order derivative) as its first truncated term. An even order derivative term, with proper sign, behaves like an artificial viscosity terms which helps in damping disturbances whereas an odd order derivative term disperses the disturbances without damping their magnitudes [38].
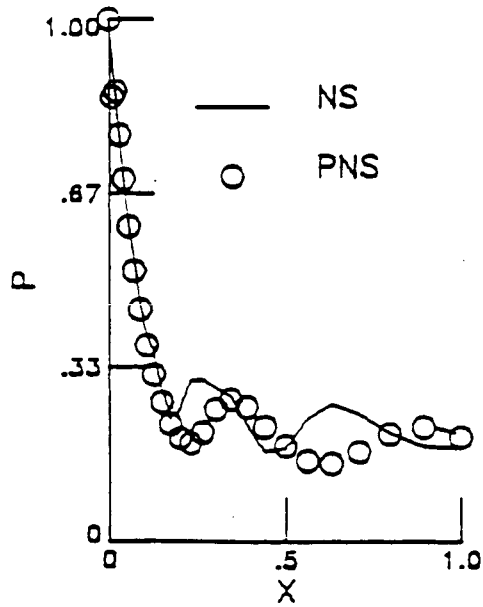
Figure 4.27 shows the results by using $C_c = 0.2$. The cross stream pressure at x-station No. 70 and the surface pressure are slightly dissipative in comparison with their three point backward counterpart in Fig.
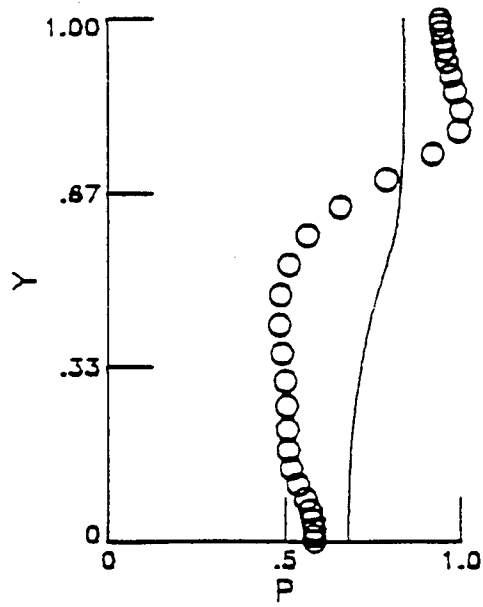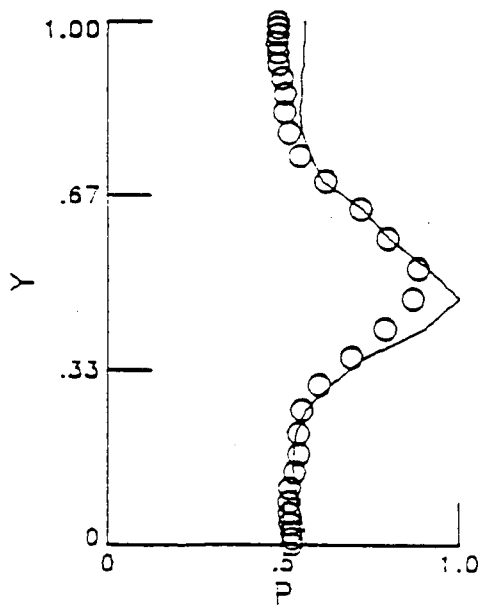
(c) P AT XST=70

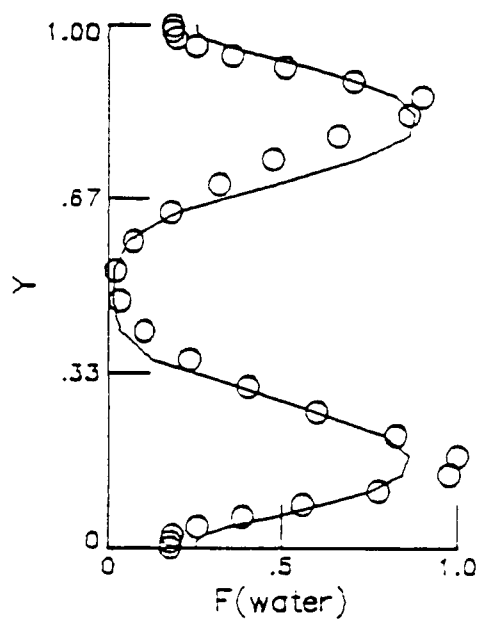(d) H$_2$O AT XST=70

(a) SURFACE P

(b) P AT XST=85

a=1, b=0.5, C$_I$=0.25, C$_E$=0.125, C$_C$=0.2

Fig. 4.24 Results of three-point-backward scheme (No. 2).

(c) P AT XST=70

(d) H_2O AT XST=70

(a) SURFACE P

(b) P AT XST=85

$a=1$, $b=0.5$, $C_1=0.50$, $C_E=0.187$, $C_C=0.0$

Fig. 4.25 Results of three-point-backward scheme (No. 3).

(c) P AT XST=70

(d) H_2O AT XST=70

NS

PNS
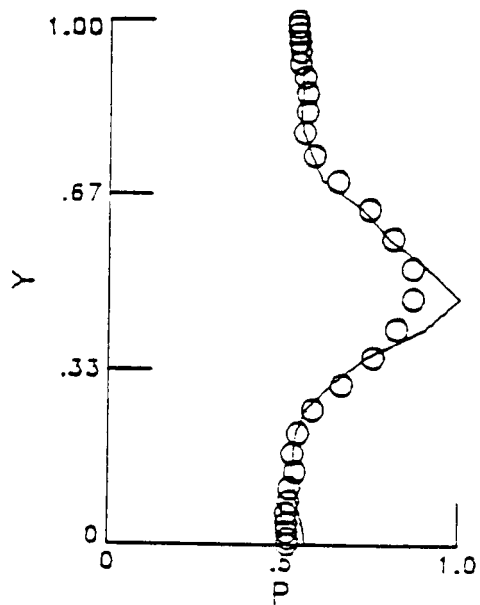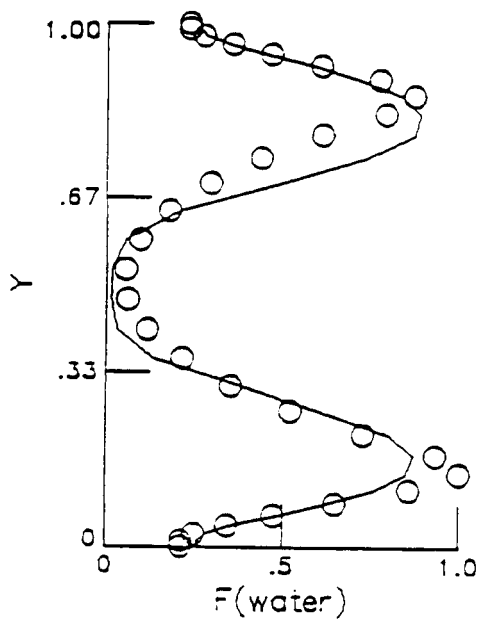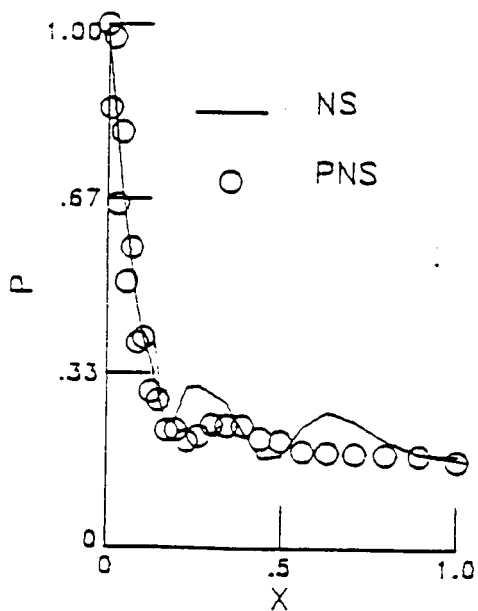
(a) SURFACE P

(b) P AT XST=85

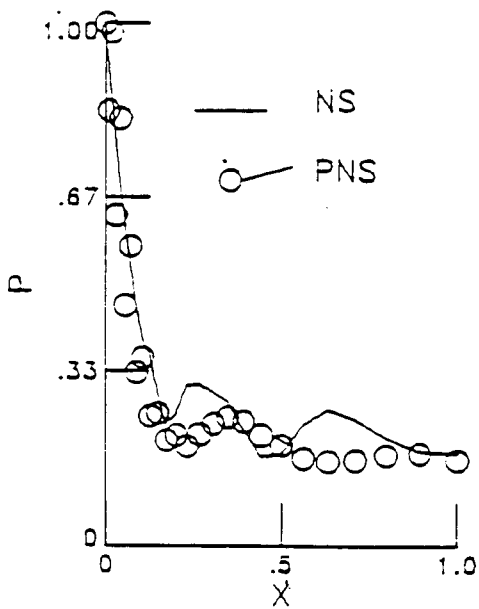$a=1$, $b=0.5$, $C_I=1.0$, $C_E=0.312$, $C_C=0.0$

Fig. 4.26 Results of three-point-backward scheme (No. 4).
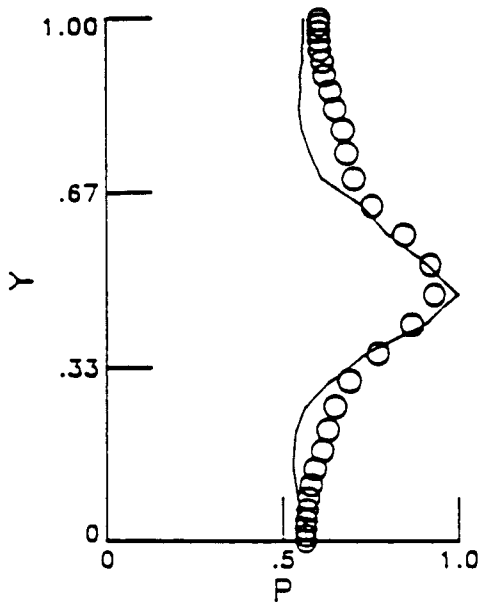
(c) P AT XST=70
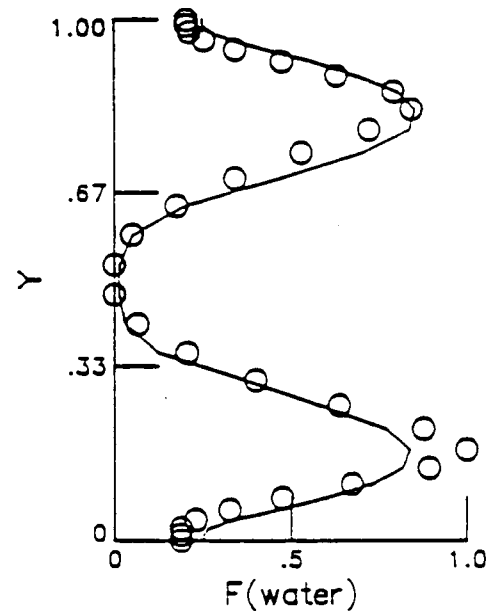
(d) H$_2$O AT XST=70
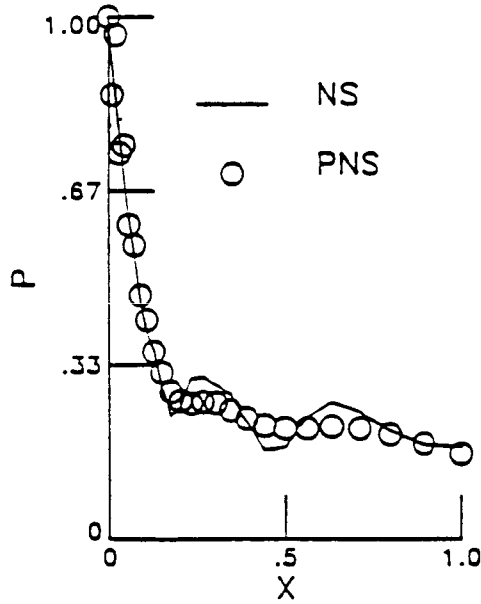
(a) SURFACE P

(b) P AT XST=85

$a=1$, $b=0$, $C_I=0.25$, $C_E=0.125$, $C_c=0.2$

Fig. 4.27 Results of Euler implicit scheme (No. 1).
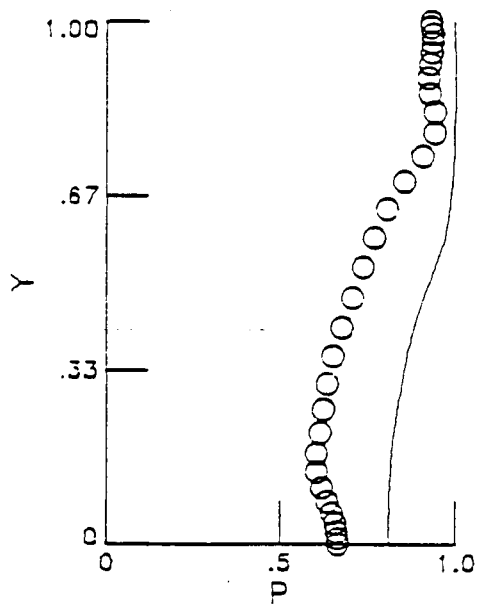
(c) P AT XST=70

(d) H$_2$O AT XST=70
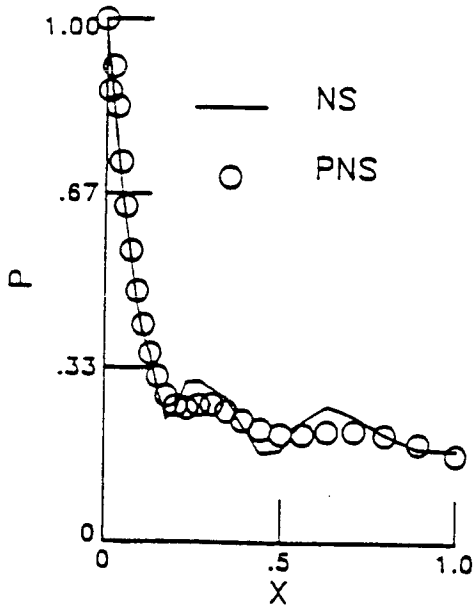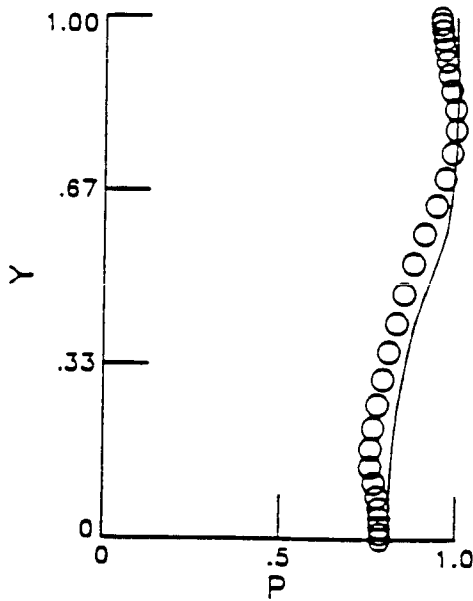
(a) SURFACE P

(b) P AT XST=85

$a=1$, $b=0$, $C_i=0.25$, $C_E=0.125$, $C_c=0.5$

Fig. 4.28 Results of Euler implicit scheme (No. 2).

(c) P AT XST=70

(d) H$_2$O AT XST=70

NS

○ PNS
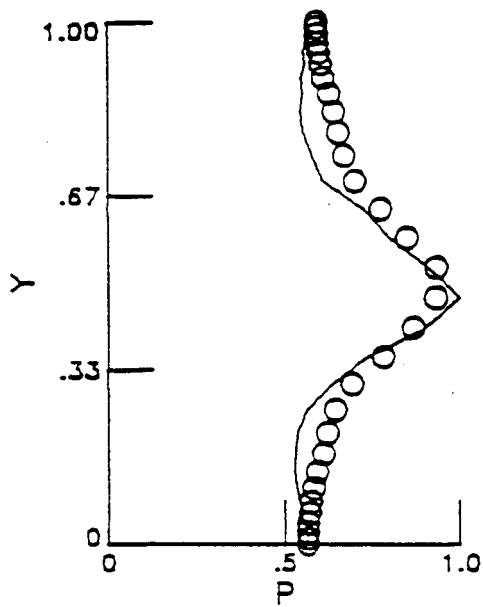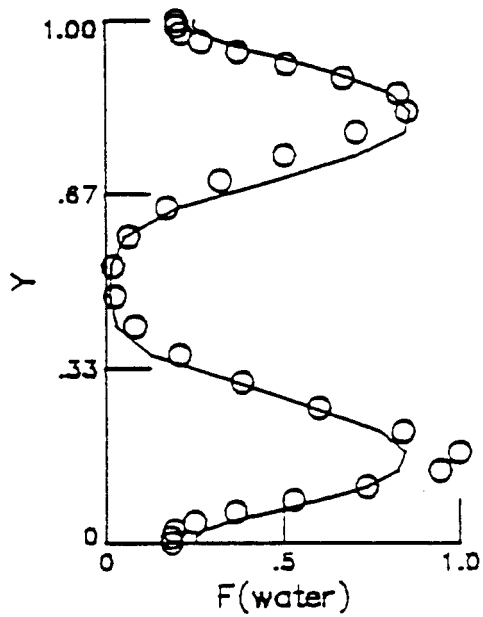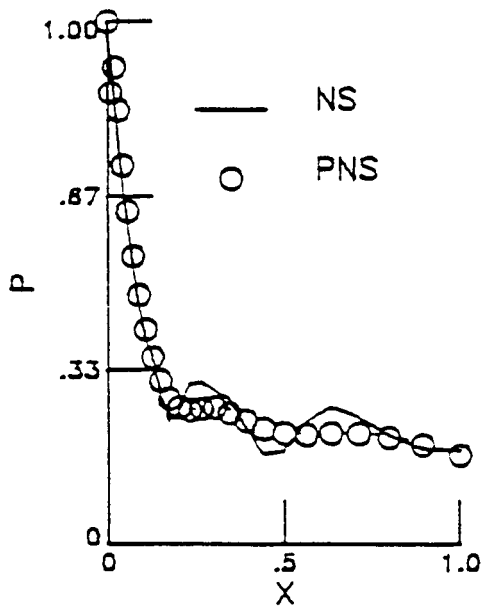
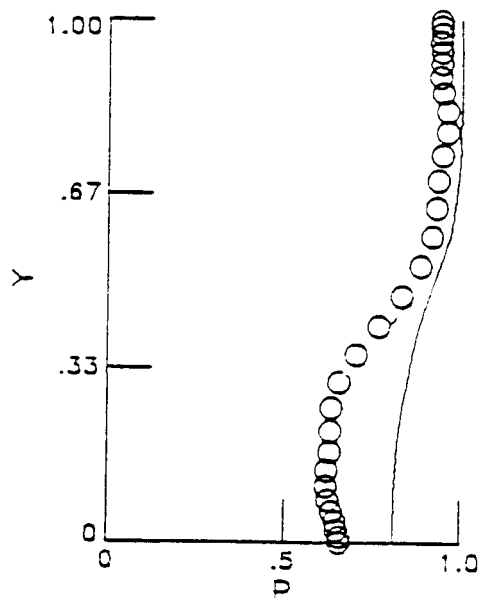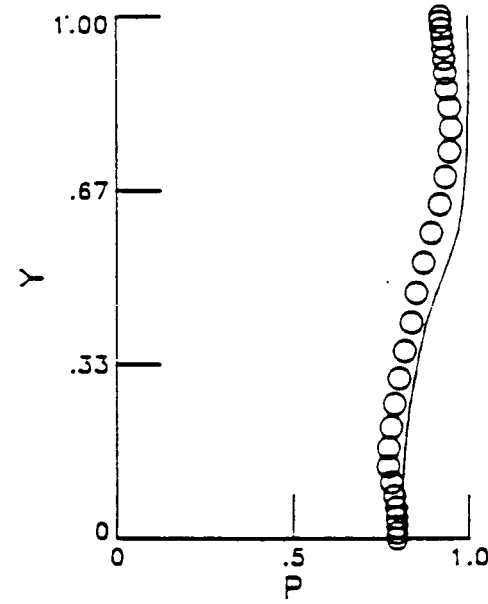(a) SURFACE P
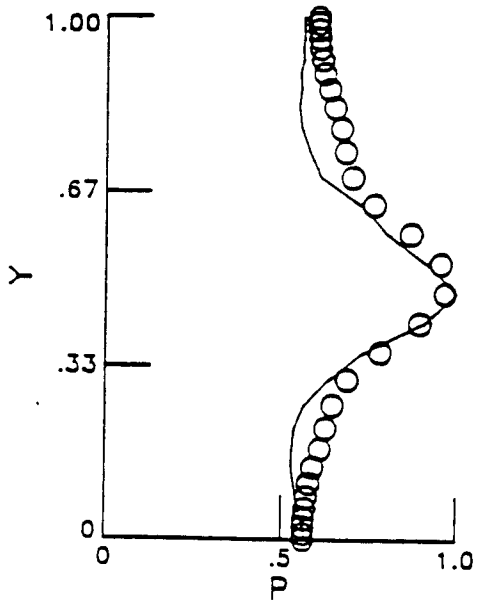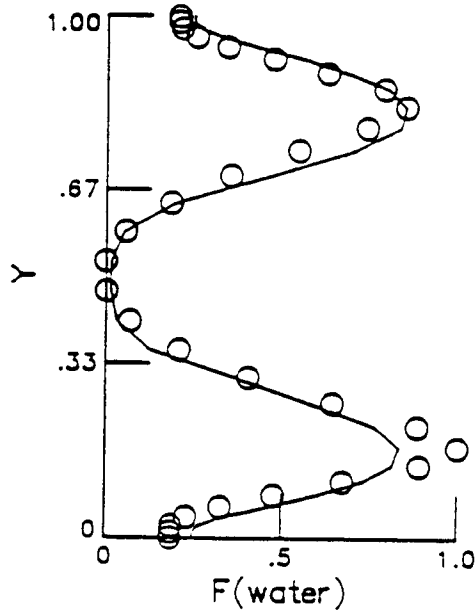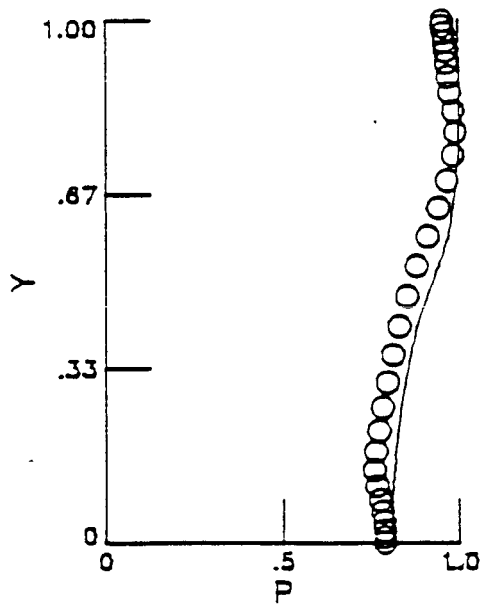
(b) P AT XST=85

a=1, b=0, C$_I$=0.50, C$_E$=0.187, C$_c$=0.5

Fig. 4.29 Results of Euler implicit scheme (No. 3).

C-2

4.23. The pressure at x-station No. 85, however, compares more favorably with the NS results. The solution is further improved by increasing C_c to 0.5 as is seen in Fig. 4.28. Larger values of C_I and C_E do not seem to affect the quality of the solution (Fig. 4.29).

5. CONCLUDING REMARKS

Two computer programs for solving viscous supersonic chemically reacting flow problems associated with the hydrogen-air system have been developed. In the first computer code, the unsteady form of the fully elliptic governing equations are employed in order to capture strong upstream interactions of the flow. The finite rate global two-step chemistry model is used to represent hydrogen-air combustion. The stiffness resulting from using the chemistry model is circumvented by evaluating the chemistry source terms implicitly. The elliptic code is written in a vector FORTRAN language which is made operational only on the VPS-32 vector processing computer at the NASA-LaRC. The fluid dynamics part of the governing equations is integrated in time by a fully explicit MacCormack algorithm. Due to implicit source terms, the chemistry part of the governing equations gives rise to a block monodiagonal system of algebraic equations which can be solved also in a vectorized manner giving considerable saving in computer time over a scalar inversion procedure. The results obtained from the elliptic code in solving two internal flow problems are physically reasonable. In the case of the scramjet inlet-combustor configuration problem, the code predicts strong interactions between the inlet and the combustor which could choke the flow in the inlet.

The second computer code employs a parabolized form of the governing equations in which only a fraction of the streamwise pressure gradient is

retained. The code is applicable for supersonic high Reynolds number flows with weak upstream interaction such as regions far downstream of the transverse fuel injector in a scramjet engine. The governing equations are solved in a fully coupled fully implicit manner in order to capture strong shock waves as well as fluid-chemistry interactions. The finite difference algorithm used is fairly general; it degenerates into many familiar schemes upon specifying two parameters. The fully coupled procedure yields a block (8x8) tridiagonal system of algebraic equations which is solved by a noniterative method. Solution is obtained by forward marching in the streamwise spatial direction only one time providing considerable saving in computer resources when compared with the elliptic code. If desired, a multi-sweep procedure can be devised with minimal effort. The results obtained from the parabolized code compare reasonably well with those from the elliptic results. The first order accurate Euler implicit scheme is found to give good results. In some cases, the Euler implicit scheme gives even better results than the second order accurate three point backward scheme. In a real application, it is highly desirable to have a bench mark solution to compare results of the three point backward scheme against results of the Euler implicit scheme in order to determine which scheme is more appropriate for the class of flow being investigated. For cases where bench mark solutions are not available, the Euler implicit scheme is recommended since, in general, it should provide fairly accurate results. If the three point backward scheme is selected, the suggested values of various parameters are: C_I = 0.25, C_E = 0.125, C_c = 0.0. For the Euler implicit scheme, the following values are recommended: C_I = 0.25, C_E = 0.125 and C_c = 0.5.

The robustness of the parabolized code is considerably improved by introducing the parameter C_c into the continuity equation and the species

equations. The value of C_c = 0.2 can suppress pressure oscillation while still maintaining overall accuracy. Non-zero value of C_c, however, is recommended for a first order accurate scheme only since it could disrupt the formal accuracy of higher order schemes.

The results of the two problems solved by the present parabolized algorithm confirm that the algorithm is highly conservative. Regardless of the quality of the solution, mass flow rate across the channel at all stations are always within 0.01 percent of one another.

Further investigations are obviously needed in the area of turbulent jet mixing. The algebraic turbulence model used in this study serves only as a starting point. The multi-component mass diffusion processes also need more elaboration. In any event, experimental data are highly desirable to validate the models. More sophisticated finite rate chemistry models can be included especially in the parabolized formulation. Inclusion of better chemistry models always means more species and more reaction paths; this makes the elliptic equation approach very expensive.

REFERENCES

1. Henry, J. R. and Anderson, G. Y., "Design Considerations for the Air-frame-Integrated Scramjet," NASA TM X-2895, Dec. 1973.

2. Anderson, G. Y., "Hypersonic Propulsion," NASA SP-381, 1975, pp. 459-474.

3. Jones, R. A. and Huber, P. W., "Toward Scramjet Aircraft," Astronautics and Aeronautics, Vol. 16, Feb. 1978, pp. 38-48.

4. Beach, H. L., Jr., "Hypersonic Propulsion," NASA CP-2092, May 1979, pp. 387-407.

5. Kumar, A., "Numerical Analysis of the Scramjet Inlet Flow Field Using Two-Dimensional Navier-Stokes Equations," NASA TP 1940, Dec. 1981.

6. Kumar, A. and Tiwari, S. N., "Analysis of the Scramjet Inlet Flow Field Using Two-Dimensional Navier-Stokes Equations," NASA CR 3562, June 1982.

7. Kumar, A., "Numerical Analysis of a Scramjet Inlet Flow Field Using the Three-Dimensional Navier-Stokes Equations," presented at the JANAF Propulsion Meeting, Feb. 1983.

8. Chitsomboon, T. and Tiwari, S. N., "A Second-Order Accurate Parabolized Navier-Stokes Algorithm for Internal Flows," NASA CR 174258, Nov. 1984.

9. Chitsomboon, T., Kumar, A., and Tiwari, S. N., "A Parabolized Navier-Stokes Algorithm for Separated Supersonic Internal Flows," AIAA Paper No. 85-1411, July 1985.

10. Drummond, J. P., "Numerical Investigation of Perpendicular Injector Flow Field in a Hydrogen Fueled Scramjet," AIAA Paper No. 79-1483, 1979.

11. Weidner, E. H. and Drummond, J. P., "Numerical Study of Staged Fuel Injection for Supersonic Combustion," AIAA Journal, Vol. 20, No. 10, Oct. 1982, pp. 1426-1431.

12. Dwyer, H. A. and Sander, B. R., "Numerical Modeling of Unsteady Flame Propagation," Acta Astronautica, Vol. 5, Nov. 1978, pp. 1171-1184.

13. Kee, R. J. and Dwyer, H. A., "Review of Stiffness and Implicit Finite-Difference Methods in Combustion Modeling," Progress in Astronautics and Aeronautics, Vol. 76, 1979, pp. 485-500.

14. Williams, F. A., Combustion Theory, Addison-Wesley, Massachusetts, 1965.

15. Strehlow, R. A., Combustion Fundamentals, McGraw-Hill, New York, 1984.

16. Rogers, R. C. and Schexnayder, C. J., Jr., "Chemical Kinetic Analysis of Hydrogen-Air Ignition and Reaction Time," NASA TP 1856, 1981.

17. Evans, J. S. and Schexnayder, C. J., Jr., "Influence of Chemical Kinetic and Unmixedness on Burning in Supersonic Hydrogen Flames," AIAA Journal, Vol. 18, No. 2, Feb. 1980, pp. 188-193.

18. Rogers, R. C. and Chinitz, W., "Using a Global Hydrogen-Air Combustion Model in Turbulent Reacting Flow Calculation," AIAA Journal, Vol. 20, No. 4, April 1983, pp. 586-592.

19. Bui, T. D., Oppenheim, A. K., and Pratt, D. T., "Recent Advances in Methods for Numerical Solution of O.D.E. Initial Value Problems," Lawrence Berkeley Laboratory Report No. LBL-16943, Dec. 1983.

20. Pratt, D. T., "Exponential-Fitted Methods for Integrating Stiff Systems of Ordinary Differential Equations," Applications to Homogeneous Gas-Phase Chemical Kinetics," Presented at JANAF Propulsion Meeting, New Orleans, LA, Feb. 1984.

21. Drummond, J. P., Hussaini, M. Y., and Zang, T. A., "Spectral Methods for Modeling Supersonic Chemically Reacting Flow Fields," ICASE Report No. 85-20, Institute for Computer Applications in Science and Engineering, Hampton, VA, March 1985.

22. Aiken, R. C., (Editor), Stiff Computation, Oxford University Press, 1985.

23. Hindmarsh, A. C. and Byrne, G. D., "EPISODE: An Effective Package for the Integration of System of Ordinary Differential Equations," UCID Report No. 30112, Lawrence Livermore Laboratory, 1977.

24. Hindmarsh, A. C., "LSODE and LSODI, Two New Initial Value Ordinary Differential Equations Solvers," SIGNUM Newsletter, Vol. 15, No. 4, Dec. 1980, pp. 10-11.

25. Gear, C. W., Numerical Initial Value Problems in Ordinary Differential Equations, Prentice-Hall, 1971.

26. Gear, C. W., "The Automatic Integration of Ordinary Differential Equations," Communications of the ACM, Vol. 14, No. 3, 1971, pp. 176-179.

27. Eklund, D. R., Hassan, H. A., and Drummond, J. P., "The Efficient Calculation of Chemically Reacting Flow," AIAA Paper No. 86-0563, Jan. 1986.

28. Widhopf, G. F. and Victoria, K. J., "On the Solution of the Unsteady Navier-Stokes Equations Including Multicomponent Finite Rate Chemistry," Computers and Fluids, Vol. 1, June 1973, pp. 159-184.

29. Smoot, L. D., Hecker, W. C., and Williams, G. A., "Prediction of Propogating Methane-Air Flames," Combustion and Flame, Vol. 26, June 1976., pp. 323-343.

30. Stalnaker, J. F., Robinson, M. A., Spradley, L. W., Kurzius, S. C., and Thoenes, J., "Development of the General Interpolants Methods for the Cyber 200 Series of Computers," Report TR 0867354, Lockheed-Huntsville Research and Engineering Center, Huntsville, AL, Oct. 1983.

31. Bussing, T. R. A. and Murman, M., "A Finite Volume Method for the Calculation of Compressible Chemically Reacting Flows," AIAA Paper No. 85-0331, Jan. 1985.

32. Drummond, J. P., Hussaini M. Y., and Zang, T. A., "Spectral Methods for Modeling Supersonic Chemically Reacting Flow Fields," AIAA Paper No. 85-0331, Jan. 1985.

33. Bussing, T. R. A. and Murman, E. M., "Numerical Investigation of Two-Dimensional H_2-Air Flame Holding Over Ramps and Rearward Facing Steps," AIAA Paper No. 85-1250, July 1985.

34. Chitsomboon, T. and Tiwari, S. N., "Investigation of Chemically Reacting Supersonic Internal Flows." Department of Mechanical Engineering and Mechanics, School of Engineering, Old Dominion University. TR NAG-1-423, Sept. 1985.

35. Chitsomboon, T., Kumar, A., Drummond, J. P., and Tiwari, S. N., "Numerical Study of Supersonic Combustion Using a Finite-Rate Chemistry Model," AIAA Paper No. 86-0309, Jan. 1986.

36. Schlichting, H., Boundary-Layer Theory, 7th Ed., McGraw-Hill, New York, 1979.

37. Roache, P J., Computational Fluid Dynamics, Hermosa Publishing Corporation, Albuquerque, New Mexico, 1972.

38. Anderson, D. A., Tannehill, J. C., and Pletcher, R. H., Computational Fluid Mechanics and Heat Transfer, Hemishere Washington, 1984.

39. Ferri, A., "Review of Problems in Application of Supersonic Combustion." Journal of Royal Aeronautical Society, Vol. 68, Sept. 1964.

40. Rudman, S. and Rubin, S. G., "Hypersonic Viscous Flow Over Slender Bodies with Sharp Leading Edges," AIAA Journal, Vol. 6, Oct. 1968, pp. 1883-1889.

41. Lighthill, M. J., "On Boundary Layers and Upstream Influence Supersonic Flows without Separation," Proceedings of Royal Society of London (A), Vol. 217, 1953, pp. 478-507.

42. Lubard, S. C. and Helliwell, W. S., "Calculation of the Flow on a Cone at High Angle of Attack," AIAA Journal, Vol. 12, July 1974, pp. 965-974.

43. Chilukuri, R. and Pletcher, R. H., "Numerical Solutions to the Partially Parabolized Navier-Stokes Equations for Developing Flow in a Channel," Numerical Heat Transfer, Vol. 3, No. 2, April 1980, pp. 169-188.

44. Madavan, N. K. and Pletcher, R. H., "Prediction of Laminar Separated Flows Using the Partially Parabolized Navier-Stokes Equations," AIAA Paper No. 83-1954, 1983.

45. Ghia, U., Ghia, K. N., Rubin, S. G., and Khosla, P. K., "Study of Incompressible Flow Separation Using Primitive Variables," Computers and Fluids, Vol. 9, June, 1981, pp. 123-142.

46. Rubin, S. G., "A Review of Marching Procedures for Parabolized Navier-Stokes Equations," Numerical and Physical Aspects of Aerodynamic Flows, Springer-Verlag, 1982, pp. 171-186.

47. Rubin, S. G. and Reddy, D. R., "Global PNS Solutions for Laminar and Turbulent Flow," AIAA Paper No. 83-1911, 1983.

48. Reddy, D. R. and Rubin, S. G., "Subsonic Transonic, Viscous Inviscid Relaxation Procedures for Strong Pressure Interactions," AIAA Paper No. 84-1627, June 1984.

49. Patankar, S. V. and Spalding, D. B., "A Calculation Procedure for Heat, Mass and Momentum Transfer in Three-Dimensional Parabolic Flows," International Journal of Heat and Mass Transfer," Vol. 15, Oct. 1972, pp. 1787-1806.

50. Markatos, N. C. Spalding, D. B., and Tatchell, D. G., "Combustion of Hydrogen Injected into a Supersonic Airstream (The SHIP Computer Program)," NASA CR-2802, April 1977.

51. Drummond, J. P., Rogers, R. C., and Evans, J. S., "Combustor Modeling for Scramjet Engines," Presented at the AGARD 54th (B) Specialists Meeting on Combustor Modeling, Cologne, Germany, Oct. 1979.

52. Pan, Y. S., "The Development of a Three-Dimensional Partially Elliptic Flow Computer Program for Combustion Research," NASA CR-3057, Nov. 1978.

53. Vigneron, Y. C., Rakich, J. V., and Tannehill, J. C., "Calculation of Supersonic Viscous Flow Over Delta Wings with Sharp Subsonic Leading Edges," AIAA Paper No. 78-1137, July 1978.

54. Beam, R. M. and Warming R. F., "An Implicit Finite-Difference Algorithm for Hyperbolic Systems in Conservation-Law Form," Journal of Computational Physics, Vol. 22, Sept. 1979, pp. 87-110.

55. Briley, W. R. and McDonald, H., "On the Structure and Use of Linearized Block Implicit Schemes," Journal of Computational Physics, Vol. 34, Jan. 1980, pp. 54-73.

56. Khosla, P. K. and Lai, H. T., "Global PNS Solution for Transonic Strong Interaction Flows," AIAA Paper No. 79-0130, Jan. 1979.

57. Schiff, L. B. and Steger, J. L., "Numerical Simulation of Steady Supersonic Viscous Flow," AIAA Paper No. 79-0130, Jan. 1979.

58. Rubin, S. G. and Lin, T. C., "Numerical Methods for Two- and Three-Dimensional Viscous Flow Problems, PIBAL Report No. 71-8, Polytechnical Institute of Brooklyn, Farmingdale, N.Y., April 1971.

59. Rakich, J. V., "Iterative PNS Method for Attached Flows with Upstream Influence," AIAA Paper No. 83-1955, July 1983.

60. Reyhner, T. A. and Flügge-Lotz, I., "The Interaction of a Shock Wave with a Laminar Boundary Layer," International Journal of Non-Linear Mechanics, Vol. 3, No. 2, June 1968, pp. 173-199.

61. Spalding, D. B., Launder, B. E., Morse, A. P., and Maples, G., "Combustion of Hydrogen-Air Jets in Local Chemical Equilibrium (A Guide to the CHARNAL Computer Program)," NASA CR-2407, June 1974.

62. Dyer, D. F., Maples, G., and Spalding, D. B., "Combustion of Hydrogen Injected into a Supersonic Airstream," NASA CR-2655, March 1976.

63. Sinha, N. and Dash, S. M., "Parabolized Navier-Stokes Analysis of Ducted Turbulent Mixing Problems with Finite-Rate Chemistry," AIAA Paper No. 86-0004, Jan. 1986.

64. Kumar, A., "User's Guide to NASCRIN - A Vectorized Code for Calculating Two-Dimensional Supersonic Internal Flow Fields," NASA TM 85708, Feb. 1984.

65. Baldwin, B. S. and Lomax, H., "Thin Layer Approximation and Algebraic Model for Turbulent Flows," AIAA Paper No. 78-257, Jan. 1978.

66. Peters, G. R., Agarwal, R. K., and Deese, J. E., "Numerical Simulation of Several Shock-Separated Boundary-Layer Interaction Flows Using Zero- and Two-Equation Turbulence Models," AIAA Paper No. 86-0248, Jan. 1986.

67. McBride, B. J., Heimel, S., Ehlens, J. G., and Gordon, S., "Thermodynamic Properties to 6000 K for 210 Substances Involving the First 18 Elements," NASA SP-3001, 1963.

68. MacCormack, R. W., "The Effect of Viscosity in Hypervelocity Impact Cratering," AIAA Paper No. 69-354, May 1969.

69. MacCormack, R. W. and Baldwin, B. S., "A Numerical Method for Solving the Navier-Stokes Equations with Application to Shock-Boundary Layer Interactions," AIAA Paper No. 75-1, Jan. 1975.

70. Drummond, J. P., Private Communication.

71. Chaussee, D. S., "NASA AMES Parabolized Navier-Stokes Code (PANS)," UTSI Publication No. E02-4005-023-84, Tullahoma, Tennessee, March 1984.

72. Srinivasan, G. R., Nicolet, W. E. and Shanks, S. P., "Viscous Hypersonic Flow Over Complex Bodies at High Angles of Attack," AIAA Paper No. 84-0015, Jan. 1984.

73. Roberts, G. O., Computational Meshes for Boundary Layer Problems, Springer-Verlag, New York, 1971, pp. 171-177.

74. Drummond, J. P. and Weidner, E. H., "Numerical Study of a Scramjet Engine Flow Field," AIAA Journal, Vol. 20, No. 9, Sept. 1982.

APPENDIX A

DERIVATION OF HEAT FLUX TERMS

Only the $\partial q/\partial x$ term will be derived here; relation for $\partial q/\partial y$ follows the same line of derivation. The heat flux term is given in its unsimplified form as

$$q_x = -k \frac{\partial T}{\partial x} - \rho D \sum_{i=1}^{5} \left[\left(\frac{\partial f_i}{\partial x} \right) h_i \right] \qquad (A.1)$$

by using the relation

$$\alpha = k/\rho \overline{C}_p \qquad (A.2)$$

and

$$Le = \alpha/D . \qquad (A.3)$$

Eq. (A.1) can be rearranged as

$$q_x = -\rho D \left\{ Le \, \overline{C}_p \frac{\partial T}{\partial x} + \sum_{i=1}^{5} \left[\left(\frac{\partial f_i}{\partial x} \right) h_i \right] \right\} \qquad (A.4)$$

with the help of the relations (A.3) and

$$Pr = \nu/\alpha \qquad (A.5)$$

the term ρD can be written as

$$\rho D = \frac{\mu}{Le \ Pr} \qquad (A.6)$$

For a unit Lewis number, Eq. (A.4) can be given as

$$q_x = - \frac{\mu}{Le \ Pr} \ [\overline{C}_p \frac{\partial T}{\partial x} + \sum_{i=1}^{5} \{(\frac{\partial}{\partial x} f_i)h_i\}] \qquad (A.7)$$

where

$$\overline{C}_p = \sum_{i=1}^{5} f_i \ C_{pi}. \qquad (A.8)$$

The static enthalpy for the mixture is given by

$$h = \sum_{i=1}^{5} f_i \ (H_i^\circ + \int_0^T C_{pi}(\xi) \ d\xi). \qquad (A.9)$$

Note that the dummy variable, ξ, is employed in evaluating the sensible enthalpy. Upon taking a partial derivative with respect to x and applying the Leibnitz rule one obtains

$$\frac{\partial h}{\partial x} = \sum_{i=1}^{5} [(H_i^\circ + \int_0^T C_{pi}(\xi) \ d\xi) \frac{\partial f_i}{\partial x} + f_i \frac{\partial H_i^\circ}{\partial x}$$

$$+ f_i \int_0^T \frac{\partial C_{pi}}{\partial x} (\xi) \ d\xi + f_i \ C_{pi} \ (T) \frac{\partial T}{\partial x}]. \qquad (A.10)$$

By realizing that the coefficient of the first term is nothing but h_i and

the second and the third terms are identically zero, Eq. (A.10) can be written as

$$\frac{\partial h}{\partial x} = \sum_{i=1}^{5} \left(\frac{\partial f_i}{\partial x}\right) h_i + \sum_{i=1}^{5} f_i C_{pi} \frac{\partial T}{\partial x} \qquad (A.11)$$

or

$$\frac{\partial h}{\partial x} = \sum_{i=1}^{5} \left(\frac{\partial f_i}{\partial x}\right) h_i + \bar{C}_p \frac{\partial T}{\partial x}. \qquad (A.12)$$

Substituting Eq. (A.12) into (A.7), the desired relation is finally obtained. It is important to note that the simplification is possible only for the unit Lewis number assumption. The simplification is useful since it helps in organizing and simplifying the coding chore and it offers some saving in computer storage because only one array, h, is needed instead of five arrays of h_i.

APPENDIX B

JACOBIAN MATRIX FOR CHEMISTRY SOURCE TERMS

Components of the Jacobian matrix for the chemistry source terms, M_{ij}, are given in this appendix. The suffixes i and j denote row and column of the matrix, respectively. Whenever a component is not given, it means that component is identically zero. It should be noted that temperature dependency of the kinetic rate terms, k_f and k_b, is not considered in evaluating the components. The temperature for these terms is simply lagged one step behind the step where solutions are being sought. The matrix takes exactly the same form for both the elliptic and the parabolized formulation but in the parabolized formulation the matrix is defined as C rather than M (see section 3.2). The components are given as follows:

$$Z = J^{n+1}/J^n$$

$$M11 = -(k_{f1}/M_3)Z\rho_3$$

$$M13 = -(k_{f1}/M_3)Z\,\rho_1$$

$$M14 = (k_{b1}\,M_1/M_4^2)Z\,\rho_4$$

$$M22 = -(4k_{b2}/M_2)Z\,\rho_2$$

$$M23 = \frac{2k_{f2}\,M_2\,Z^2\,\rho_4^2}{M_3\,M_4^2}$$

$$M24 = \frac{4k_{f2}\ M_2\ Z^2\ \rho_3\ \rho_4}{M_3\ M_4^2}$$

$$C1 = M_3/M_1$$

$$C2 = -M_3/2M_2$$

$$M31 = (C1)(M11)$$

$$M32 = (C2)(M22)$$

$$M33 = (C1)(M13) + (C2)(M23)$$

$$M34 = (C1)(M14) + (C2)(M24)$$

$$C3 = -2M_4/M_1$$

$$C4 = -M_4/M_2$$

$$M41 = (C3)(M11)$$

$$M42 = (C4)(M12)$$

$$M43 = (C3)(M13) + (C4)(M23)$$

$$M44 = (C3)(M14) + (C4)(M24)$$

APPENDIX C

VECTORIZED SUBROUTINE FOR SOLVING
A BLOCK MONO-DIAGONAL SYSTEM

The following subroutine is written in CDC CYBER 200 FORTRAN VERSION 2 (Vector FORTRAN) in order to make it operates efficiently on the VPS-32 vector processing comuter at the NASA-LaRC. The solution procedure can be made more efficient by realizing that only a fraction of mesh points are chemically reacting; the rest of the mesh points are nonreacting and can be integrated by a fully explicit procedure which is much less expensive. The reacting mesh points are distributed throughout the domain, more or less, randomly. The scalar array, (IT), and the bit array, (B2), are calculated independently in the main body of the program and are used as maps for determining which mesh points are chemically active. The sparse arrays can then be compressed into concatenate locations giving shorter vectors lengths and therefore less mathematical operations. Finally, the solution can be expanded back into their real locations with the help of the maps (IT) and (B2).

```
      SUBROUTINE LUDEC(NN)
      BIT B1,B2
      COMMON/COM1/IT(NY,NX),B2(NY,NX),Q(NY,NX,4,4),RHS(NY,NX,4)
     1,SLN(NY,NX,4),EBAR(NY,NX,4),NXM4,IRP
C
C DECOMPOSE THE ORIGINAL (Q) MATRIX TO (LU) VECTORIALLY.
C THE METHOD IS A STRAIGHT FORWARD DECOMPOSITION WITH THE
C DIAGONAL TERMS OF (L) EQUAL TO ONE.
C THE (LU) MATRIX IS STORED BACK INTO THE (Q) MATRIX.
```

```
C NOTE ALSO THAT THE SPARSE VECTORS ARE COMPRESSED INTO
C CONCATENATE VECTORS, BY THE FUNCTION "Q8VCMPRS", FOR
C EFFICIENT OPERATION.  THE COMPRESSION AND EXPANSION BACK
C INTO THE SPARSE VECTORS ARE CONTROLLED BY THE ARRAY
C (IT) AND THE BIT VECTOR (B2)
C (RHS) IS THE UNKNOWN
C (SLN) IS TEMPORARY ARRAY
C (Q)   IS THE ORIGINAL BLOCK MONO-DIAGONAL MATRIX
C IRP   IS THE LENGTH OF CONCATENATE VECTORS
C NN    IS THE DIMENSION OF THE BLOCK MATRIX
C
      NXM4=NX*NY-2*NY-2
      DO 5 I=1,NN
5     WHERE(IT(2,2;NXM4).EQ.0) SLN(2,2,I;NXM4)=RHS(2,2,I;NXM4)
C
C COMPRESS THE RHS
C
      DO 6 I=1,4
      RHS(2,2,I;NXM4)=Q8VCMPRS(RHS(2,2,I;NXM4),B2(2,2;NXM4);
     &RHS(2,2,I;NXM4))
6     CONTINUE
      DO 100 I=2,NN
      DO 110 J=1,NN
      IF(J-I)10,20,20
10    M=J-1
      IF(M)30,30,40
40    DO 50 K=1,M
```

```
50    Q(2,2,I,J;IRP)=Q(2,2,I,J;IRP)-Q(2,2,I,K;IRP)
      &*Q(2,2,K,J;IRP)

30    Q(2,2,I,J;IRP)=q(2,2,I,J;IRP)/Q(2,2,J,J;IRP)
      GO TO 110

20    M=I-1
      DO 60 K=1,M

60    Q(2,2,I,J;IRP)=Q(2,2,I,J;IRP)-Q(2,2,I,K;IRP)
      $*Q(2,2,K,J;IRP)

110   CONTINUE

100   CONTINUE

C

C SOLVE (LU)X=RHS

C X IS STORED BACK INTO RHS AND LATER ON TO SLN

C THE LAST STEP IS NOT NECESSARY, I.E., THE FINAL RHS

C CAN BE USED AS THE FINAL SOLUTION.

C

C SOLVE (L)X*=RHS

C

105   DO 200 M=2,NN
      N=M-1
      DO 140 K=1,N

140   RHS(2,2,M;IRP)=RHS(2,2,M;IRP)-RHS(2,2,K;IRP)*Q(2,2,M,K;IRP)

120   CONTINUE

200   CONTINUE

C

C SOLVE (U)X=X*

C
```

```fortran
      DO 300 M=NN,1,-1
      IF(M-NN)320,310,310
320   N=M+1
      DO 330 K=NN,N-1
330   RHS(2,2,M;IRP)=RHS(2,2,M;IRP)-RHS(2,2,K;IRP)*Q(2,2,M,K;IRP)
310   RHS(2,2,M;IRP)=RHS(2,2,M;IRP)/Q(2,2,M,M;IRP)
300   CONTINUE
C
C EXPAND BACK THE SOLUTION INTO (SLN)
C
      DO 340 I=1,4
      EBAR(2,2,I;NXM4)=Q8VXPND(RHS(2,2,I;NXM4),B2(2,2;NXM4);
     &EBAR(2,2,I;NXM4)
      WHERE (IT(2,2;NXM4).EQ.1)SLN(2,2,I;NXM4)=EBAR(2,2,I;NXM4)
350   CONTINUE
      RETURN
      END
```